A Study of Spin Precession Effects of Axisymmetric Black Holes

By

Muhammad Tabassum Riaz

NATIONAL UNIVERSITY OF MODERN LANGUAGES
ISLAMABAD
30 October 2025

A Study of Spin Precession Effects of Axisymmetric Black Holes

By

Muhammad Tabassum Riaz

MS-Math, National University of Modern Languages, Islamabad, 2025

A THESIS SUBMITTED IN PARTIAL FULFILMENT OF

THE REQUIREMENTS FOR THE DEGREE OF

MASTER OF SCIENCE

In **Mathematics**

To

FACULTY OF ENGINEERING & COMPUTING

NATIONAL UNIVERSITY OF MODERN LANGUAGES ISLAMABAD

THESIS AND DEFENSE APPROVAL FORM

The undersigned certify that they have read the following thesis, examined the defense, are satisfied with overall exam performance, and recommend the thesis to the Faculty of Engineering and Computing for acceptance.

Thesis Title: A Study of Spin Precession Effects of Axisymmetric Black Holes

Submitted By: Muhammad Tabassum Riaz **Registration #:**48 MS/MATH/S22

Master of Science in Mathematics

Title of the Degree

Mathematics

Name of Discipline

Dr. Muhammad Rizwan

Name of Research Supervisor

Signature of Research Supervisor

Dr. Anum Naseem

Name of HOD (Mathematics)

Signature of HOD (Math)

Dr. Noman Malik

Name of Dean (FEC)

Signature of Dean (FEC)

30 October, 2025

AUTHOR'S DECLARATION

I Muhammad Tabassum Riaz

Son of Riaz Hussain

Discipline Mathematics

Candidate of Master of Science in Mathematics at the National University of Modern Languages do hereby declare that the thesis A Study of Spin Precession Effects of Axisymmetric Black Holes submitted by me in partial fulfillment of MS Math degree, is my original work and has not been submitted or published earlier. I also solemnly declare that it shall not, in the future, be submitted by me for obtaining any other degree from this or any other university or institution. I also understand that if evidence of plagiarism is found in my thesis/dissertation at any stage, even after the award of a degree, the work may be canceled and the degree revoked.

Signature of Candidate

Muhammad Tabassum Riaz

Name of Candidate

30 October, 2025

Date

ABSTRACT

Title: A Study of Spin Precession Effects of Axisymmetric Black Holes

Recent advances in gravitational theory and cosmology have emphasized the need to explore black hole structures within extended frameworks beyond general relativity. This thesis investigates the spin precession effects induced by both spacetime rotation and curvature in two distinct black hole models: a rotating black hole in Brans–Dicke (BD) gravity, which includes a dynamical scalar field, and a rotating black hole surrounded by a string cloud in the presence of dark energy. The study aims to understand how spin precession behaves in these modified gravitational settings and how it can serve as a tool to distinguish between black holes and naked singularities.

By analyzing the precession of a test gyroscope near the central object, it is found that divergent precession frequencies are indicative of black hole horizons, while finite precession rates point toward naked singularities. This establishes spin precession as a potential observational criterion for differentiating these two types of compact objects. Furthermore, the influence of scalar fields and exotic matter components, such as dark energy and string clouds, on the precession behavior is explored, offering new insights into how such fields affect the spacetime geometry and the motion of spinning test particles. Overall, the results contribute to a deeper theoretical understanding of compact object classification in alternative gravity theories through physically measurable quantities.

TABLE OF CONTENTS

LIST OF FIGURES

LIST OF ABBREVIATIONS

BH	-	Black Hole
SBH	-	Schwarzschild Black Hole
KBH	-	Kerr Black Hole
RNBH	-	Reissner–Nordström Black Hole
KNBH	-	Kerr-Newman Black Hole
KLBH	-	Kerr Like Black Hole
NS	-	Naked Singularity
GR	-	General Relativity
EFE	-	Einstein Field Equations
LT	-	Lense-Thirring Precession
ZAMO	-	Zero Angular Momentum Observer
BD-Theory	-	Brans-Dicke Theory

ACKNOWLEDGMENT

First of all, I wish to express my gratitude and deep appreciation to Almighty Allah, who made this study possible and successful. This study would not have been accomplished without the honest espousal was extended from several sources, for which I would like to express my sincere thankfulness and gratitude. Yet, there were significant contributors to my attained success, and I cannot forget their input, especially my research supervisor, Dr. Muhammad Rizwan, who did not leave any stone unturned to guide me during my research journey. I really appreciate our HOD, Dr. Anum Naseem, providing us with a research environment and kind support. I really want to say thanks to our respected teachers, Dr. Sadia Riaz, Dr. Hadia Tariq, Dr. Kamran Qadir, Dr. Ghulam Murtaza and other teachers, for their guidance and support.

I shall also acknowledge the extended assistance from the administration of the Department of Mathematics, who supported me all through my research experience and simplified the challenges I faced. For all whom I did not mention but shall not neglect their significant contribution, thanks for everything.

DEDICATION

This thesis work is dedicated to my parents, family, and my teachers throughout my education career who have not only loved me unconditionally but whose good examples have taught me to work hard for the things that I aspire to achieve.

CHAPTER 1

INTRODUCTION

1.1 Einstein's Theory of Gravity

In Newtonian gravity, time is regarded as a universal and absolute quantity that remains the same for all observers, regardless of their speed or position in space. Therefore, Newton's theory of gravity is based on a three-dimensional framework in which all events occur. Isaac Newton presented the law of gravity, which states that all objects in the universe with mass attract one another. Further, the force depends on the masses of the objects and the distance between them. Newton's law of gravity was accepted for over two centuries and proved remarkably effective in predicting the motion of most objects. It has been used successfully in various practical applications, including space missions such as those that landed astronauts on the Moon. Today, it remains widely used for many practical purposes. However, Newton's law does not explain why gravity exists; it only describes the apparent effects of gravity on objects. According to Newton's theory, the gravitational force between two objects increases with their masses and decreases as the distance between them becomes larger. This force acts along the straight line joining their centres of mass. Mathematically, we can express the force F as [1]

$$F = G\frac{M_1 M_2}{r^2}, \tag{1.1}$$

where G is Newton's gravitational constant, M_1 and M_2 represent the masses of the objects, and r represents the distance between their centres of mass. Further, according to Newton's theory of gravity, time is a universal quantity; that is, it is the same for everyone, whether you are close to

a gravitational object or far from it, moving at high speed or at rest. While Newton described gravity as a law based on his observations, there are certain situations,especially under extreme conditions,where his law does not accurately explain what occurs. In science, an explanation of what consistently happens in nature is called a law.

Einstein's GR builds upon and extends Newton's theory of gravity. While Newton described gravity as a force acting at a distance between two masses, Einstein proposed a different explanation. According to him, gravity is not a force but the result of the curvature of space and time, collectively known as space-time, caused by the presence of mass and energy. His theory is based on a set of mathematical expressions called the EFE. In contrast to Newton's assumption of absolute space and time, Einstein showed that space and time are dynamic and interconnected, forming a four-dimensional spacetime. This means that time is not constant for all observers; it can vary depending on their velocity and position in a gravitational field, being affected by both motion and gravity [2, 3]. In Einstein's view, massive objects create curvature in spacetime, and this curvature determines the motion of other objects. Spacetime becomes more curved as mass increases. Although Einstein developed his theory through complex mathematical methods, a simple analogy can help illustrate it: massive objects like the Sun distort spacetime similarly to how a bowling ball deforms a stretched rubber sheet. As an object's mass increases, the curvature it causes becomes stronger. Thus, unlike Newton's view of gravitational attraction, Einstein explained that objects move along the curved paths defined by spacetime geometry [3, 4].

Thus, unlike Newton's view of gravitational attraction, Einstein explained that objects move along the curved paths defined by spacetime geometry. The amount of curvature depends on the distribution of mass-energy in spacetime. To describe this relationship mathematically, Einstein formulated the EFE, which provides the foundation of his theory. These EFE can be expressed in tonsorial form, as follows [3, 4]

$$R_{\alpha\beta} - \frac{1}{2}Rg_{\alpha\beta} = kT_{\alpha\beta}, \tag{1.2}$$

with $\alpha, \beta = 0, 1, 2, 3$ and R and $R_{\alpha\beta}$ represent the Ricci scalar and Ricci tensor, respectively, $g_{\alpha\beta}$ denotes the metric tensor of spacetime, $T_{\alpha\beta}$ represents the stress-energy tensor, and $k = 8\pi G/c^4$ is the Einstein constant. These equations show how the curvature of spacetime (given by $R_{\alpha\beta} - 1/2Rg_{\alpha\beta}$) is influenced by the presence of matter and energy (represented by the stress-energy tensor $T_{\alpha\beta}$). In simple terms, they relate the geometry of spacetime to its physical content. The EFE are a set of ten interrelated differential equations that determine how mass and energy tell spacetime how to curve, and how this curvature affects the motion of objects. John Archibald

Wheeler summarized this as: *"Spacetime tells matter how to move; matter tells spacetime how to curve"* [3].

The EFE establish a deep analogy with Maxwell's equations, which relate electromagnetic fields to electric charges and currents. Similarly, the EFE related the geometry of spacetime to the distribution of mass, energy, momentum, and stress. Given a distribution of stress-energy, the EFE can be used to determine the spacetime metric $g_{\mu\nu}$, just as Maxwell's equations determine electromagnetic fields from charge and current distributions.

The connection between the metric and curvature tensors expressed through the EFE can be written as a system of partial differential equations. If we know the mass-energy distribution in the spacetime, solutions to these equations yield the components of the metric tensor, which in turn determine the spacetime geometry. Once the geometry is known, the geodesic equation can be applied to determine the trajectories of particles and radiation [3]. Similarly, if we know the curvature of spacetime, we can obtain the mass-energy that is producing the given curvature.

The EFE are consistent with the principle of local conservation of energy and momentum, that is, in the weak gravitational fields approximation and slow-motion conditions (velocities significantly less than the speed of light, that is, $v/c \to 0$), they reduce to Newton's law of gravitation, thereby recovering classical gravity as an approximation.

Exact solutions to the EFE are rare and often require assumptions of symmetry and other simplifications. Nevertheless, these equations can describe a wide range of gravitational phenomena, including rotating BHs, gravitational waves, and the expanding universe. By further assuming small deviations from flat spacetime, the **linearized EFEs** can be derived [3]. These simplified forms are particularly useful in the study of gravitational waves and related phenomena.

1.2 Black Hole

The minimal velocity needed for any non-propelled object to escape from a gravitational body's field is called the *escape velocity*. The escape velocity v_{esc} of a gravitational object with mass M at a point P, located at a distance r from its center of mass, can be determined using the following condition:

$$\text{Kinetic energy} + \text{Gravitational potential energy} = 0 \tag{1.3}$$

which can also be written as

$$\frac{1}{2}mv_{\text{esc}}^2 - \frac{GMm}{r} = 0. \tag{1.4}$$

Solving for v_{esc}, we get:

$$\frac{1}{2}mv_{\text{esc}}^2 = \frac{GMm}{r},$$

which simplifies to:

$$v_{\text{esc}} = \sqrt{\frac{2GM}{r}}. \tag{1.5}$$

The above formula for the escape velocity shows that the escape velocity, v_{esc}, is independent of the object's mass m. The escape velocity depends only on the mass M of the central object and the distance r from its center. Therefore, the escape velocity increases with the square root of mass and decreases with the square root of distance from the center. For example, the Earth's surface its value is 11.186 km/s, whereas at the surface of the Sun it is about 617.5 km/s.

In 1784, John Michell wrote a letter to Henry Cavendish suggesting the possibility of "dark stars" in our universe. These stars possessing enough mass and extreme density can have a surface escape velocity that exceeds the speed of light. As a result, no light could escape from them, making them invisible to us. However, they could still be detected due to their strong gravitational influence on nearby objects [5]. In addition to John Michell's suggestion, a similar idea was proposed by the French mathematician and astronomer Pierre-Simon Laplace. In 1796, Laplace speculated in his work "Exposition du Système du Monde" that there could be objects in the universe with such strong gravitational fields that not even light could escape from them While he did not directly use the term "BH," Laplace's idea closely mirrored Michell's concept of "dark stars" [6, 7]. Laplace believed that these objects, if they existed, would be completely invisible, yet their presence could be inferred by their gravitational effects on nearby bodies. Laplace's work contributed to the early theoretical foundations of BH physics, even though the concept was not fully developed until the 20th century, after Einstein's theory of general relativity provided a framework for understanding such extreme gravitational phenomena [8].

A BH is an extremely dense object whose escape velocity is greater than that of the speed of light, meaning that nothing, not even light, can escape its gravitational pull. The concept of the BH plays a crucial role in testing Einstein's theory of general relativity, which, as discussed earlier, describes the relationship between mass, space, and time. Over the past decade, significant advancements have been made in detecting signals from BH collisions and capturing images of

the light from gas swirling around them, thereby teaching scientists much about the cosmos [9]. BHs have also played a key role in testing the predictions of general relativity.

The Universe is full of BHs, and while there are many different kinds, one of the most fundamental types is the Schwarzschild black hole(SBH), which has only one parameter: the mass. From an astronomical perspective, a BH is often considered the ultimate result of a massive star's gravitational collapse. The solution of EFE in this context initially seemed impractical. In the 1920s, it was discovered that a massive star could become a white dwarf because the degeneracy pressure of electrons would prevent the star from completely collapsing without nuclear fusion. However, Subrahmanyan Chandrasekhar proposed in 1931 that if the mass of a star exceeds a certain limit, known as the Chandrasekhar limit (about 1.44 times the mass of the Sun), the degeneracy pressure of electrons would no longer be able to stop the star from collapsing further [10, 11]. This theory was initially rejected by many scientists, including Arthur Eddington, who thought some other force could halt the collapse. Later, it was discovered that a neutron star could form from a star's collapse above the Chandrasekhar limit, halting the collapse at that moment [10].

Albert Einstein himself rejected the idea of BHs in 1939, stating that it was not feasible for stars to shrink to zero size and that no astronomical object could have such a strong gravitational pull that even light could not escape from it [12]. Despite Einstein's rejection, J. R. Oppenheimer and H. S. Snyder in 1939 showed through their work on gravitational collapse that BHs could indeed form [13, 14], though they suggested that no observable effects could be detected with the telescopes of the time.

The idea of BHs gained more credence in the 1950s when quasars, extremely bright active galactic nuclei, were discovered. Initially, it was unclear what process was responsible for generating quasars, but in 1964, Edwin Salpeter and Yakov Zel'dovich separately postulated that quasars might be fueled by a binary hypernova extracting material from a nearby massive star, forming an accretion disk [15, 16]. In 1964, the first BH was identified as Cygnus X-1, with its mass determined to be more than a neutron star as suggested by the study of its orbital motion [17]. This discovery led scientists to acknowledge the existence of BHs in the universe. Advancements in technology have furthered BH astrophysics. The detection of gravitational waves by LIGO and Virgo, which result from the merger of two BHs, has opened up new avenues of study [18, 19]. In 2019, the first-ever image of a supermassive BH at the center of galaxy M87 was captured using the Event Horizon Telescope. This BH has a mass approximately 6.5 billion

times that of the Sun [9]. These findings have provided new insights into the various facets of BHs and have resolved long-standing debates regarding their existence, offering support for the predictions made by Newton's and Einstein's theories of gravity. Through these observations and discoveries, BHs have not only tested Einstein's GR but have also deepened our understanding of space, time, and gravity.

1.3 Naked Singularity

Relativistic astrophysics and gravitational theory are profoundly concerned with the gravitational collapse of a massive star and its eventual outcome. When a giant star exhausts its nuclear fuel, the gravitational force of the star's own mass overcomes the internal pressure that was previously counteracting the collapse. As a result, the star begins to collapse, becoming denser and denser under the dominance of gravity. The ultimate fate of this collapse depends on the star's initial mass. For stars with a mass less than three times that of the Sun, the collapse will likely end in the formation of a white dwarf or a neutron star. However, for significantly more massive stars, the collapse continues, eventually leading to the formation of a spacetime singularity [20].

A spacetime singularity represents a point where the curvature of spacetime becomes infinite, and physical quantities such as mass and energy lose their well-defined meaning, making the laws of physics no longer applicable. According to the uniqueness theorem of general relativity, a singularity can either be visible to external observers, in which case it is called a NS, or it can be hidden behind the event horizon of a BH, making it invisible to the observer outside the BH [3, 21]. Thus, we define the event horizon as a trapping boundary beyond which nothing, not even light, can escape the BH's due to the gravitational pull. In the case of a BH, the singularity is enclosed and hence covered by the event horizon, rendering it undetectable to any external observers.

The nature of the collapsing star's internal dynamics determines whether the singularity becomes a NS or is covered and by the the event horizon of a BH. If the final outcome of the star's collapse is a BH, the event horizon serves as the defining feature of the BH, marking the boundary beyond which any information or matter cannot escape. The event horizon of a black hole is a crucial surface, playing a significant role in distinguishing between two possible

outcomes: a black hole with a hidden singularity or a naked singularity that challenges the predictions of general relativity.

In this thesis, we explore both scenarios, focusing on how the spin precession frequency of the axis of a sniping test gyroscope can serve as a tool to differentiate between naked singularities (NSs) and Kerr-like BHs [22]. This distinction is central to understanding the nature of gravitational collapse and the boundary conditions of spacetime singularities.

1.4 Types of Black Hole

If a spacetime admits the timelike Killing vector ∂_t, it is considered stationary. This indicates that $\partial g_{\mu\nu}/\partial t = 0$, which mean the metric components $g_{\mu\nu}$ are independent of t. If the metric of a stationary spacetime remains unchanged when the time coordinate t is changed to $-t$, it is referred to as static. If the metric components of a spacetime does no change by changing the azimuthal angle coordinate ϕ around the axis of symmetry, meaning that $\partial g_{\mu\nu}/\partial \phi = 0$, this spacetime is considered axisymmetric. Based on the conditions outlined above, if all components of the metric are independent of both time (t) and the azimuthal angle (ϕ), then the following conditions must hold:

$$g_{tr} = g_{r\phi} = g_{t\theta} = g_{\theta\phi} = 0. \tag{1.4}$$

Consequently, the spacetime must be both stationary and axisymmetric. Further, if the metric has no cross term like $dtd\theta, drd\phi$, and the angular part of must be invariant under SO(3) rotations, that is, it must be of the form $a^2(r)d\Omega^2 = a^2(r)(r^2 + r^2\sin^2\theta)$.

1.5 Schwarzschild Black Hole

The Schwarzschild black hole (SBH) spacetime metric is the first solution to EFE, as presented by Karl Schwarzschild in 1916. To obtain this solution, Schwarzschild considered vacuum spacetime outside a spherically symmetric gravitational source of mass M, situated at the origin. The Schwarzschild metric is a one-parameter solution (with the parameter being the mass of the gravitational source), and it provides an excellent approximation for the gravitational field

due to non-rotating spherically symmetric gravitational source, such as a star, planet, or static BH. The line element of SBH (which gives the metric tensor) can be mathematically written as [3, 4]

$$ds^2 = -\left(1 - \frac{2GM}{c^2 r}\right) c^2 dt^2 + \frac{1}{\left(1 - \frac{2GM}{c^2 r}\right)} dr^2 + r^2 \left(d\theta^2 + \sin^2\theta \, d\phi^2\right). \tag{1.5}$$

In natural units, where $G = 1 = c$, the Schwarzschild metric simplifies to

$$ds^2 = -\left(1 - \frac{2M}{r}\right) dt^2 + \left(1 - \frac{2M}{r}\right)^{-1} dr^2 + r^2 \left(d\theta^2 + \sin^2\theta \, d\phi^2\right). \tag{1.6}$$

From the line element (1.6), we can see that the metric components g_{tt} and g_{rr} become singular at $r = 0$ and $r = 2M$. Specifically, at $r = 0$, both g_{tt} and g_{rr} become infinite, whereas at $r = 2M$, $g_{tt} = 0$ and g_{rr} becomes infinite [3, 4]. At $r = 0$, the spacetime encounters a physical singularity (also known as a crushing singularity). At this point, the spacetime curvature becomes infinite, and therefore we are unable to apply general relativity, and we say that the laws of physics break down. In contrast, another important location is at $r = 2M$, where the metric component g_{rr} becomes infinite while the curvature remains finite. This indicates that the singularity arises due to a poor choice of coordinates and is, in fact, a coordinate singularity that can be removed through a suitable coordinate transformation. Geometrically, $r = 2M$ corresponds to the event horizon of the BH. The event horizon is a null hypersurface that separates the BH's interior from the exterior.

At the event horizon, the escape velocity equals the speed of light, as we discussed earlier; this is a defining property of the event horizon. The metric defined by (1.5) is valid only in the region outside the horizon, that is, for $r > 2M$, which ensures that the spacetime lies outside the black hole. For a long time, this solution was considered non-physical; however, it is now widely accepted as describing a real, physical object known as the SBH.

The Schwarzschild solution is considered a static solution to the EFEs, as the metric components are independent of the time coordinate t, making the metric invariant under time translations. A BH that lacks both electric charge and angular momentum is known as a Schwarzschild BH or a static BH (non-rotating). The SBH is characterized by its spherical event horizon, and it serves as the prototype for other BHs. This solution can be generalized to the Reissner-Nordström black hole (RNBH) by adding the charge along with the mass of the BH.

1.6 Reissner-Nordström Black Hole

In general relativity, the inclusion of electric charge leads to spacetime geometries that extend the Schwarzschild solution by incorporating electromagnetic effects. Under the assumptions of spherical symmetry and time independence, such geometries describe non-rotating charged black holes.

The Reissner–Nordström black hole (RNBH) is specified by two physical parameters, namely the mass M and the electric charge Q. It emerges as a static and spherically symmetric solution of the Einstein–Maxwell field equations and characterizes the spacetime surrounding a non-rotating, electrically charged compact object. In spherical coordinates and natural units, the corresponding line element is given by [3, 4]

$$ds^2 = -f(r)dt^2 + \frac{1}{f(r)}dr^2 + r^2 d\theta^2 + r^2 \sin^2\theta d\phi^2. \tag{1.7}$$

where

$$f(r) = 1 - \frac{2M}{r} + \frac{Q^2}{r^2}. \tag{1.7}$$

The electromagnetic field at every location in space is described by the four-potential

$$A^\mu = \left(\frac{Q}{r}, 0, 0, 0\right). \tag{1.8}$$

Note that, unlike the SBH, the RNBH has two horizons, called the inner and outer horizons, denoted by $r_\pm$. These horizons lie where the radial component of the metric, g_{rr}, goes to zero [11]. These horizons are located at

$$r_\pm = M \pm \sqrt{M^2 - Q^2} \tag{1.9}$$

Now, the quantity inside the square root indicates two possibilities: (i) $Q \leq M$, which makes the expression non-negative and hence $r_\pm$, and (ii) $Q < M$ and hence no real $r_\pm$. For $Q \leq M$, the condition $M = Q$ represents an extremal BH with a single event horizon. If $Q > M$, the solution corresponds to an NS. The line element in Eq. (1.7) exhibits a coordinate singularity at the RNBH horizons, $r_\pm$, and an essential singularity at $r = 0$, where the spacetime geometry becomes undefined. In the case where $Q = 0$, the RNBH reduces to the SBH.

The study of distinguishing BHs from naked singularities is an ongoing topic of research, as this distinction helps understand the nature of spacetime singularities. The Reissner-Nordström BH's horizons and singularity are key aspects in this ongoing study of BH and singularity classification [4].

1.7 Kerr Black Hole

Roy Kerr derived in 1963 the vacuum solution of the EFEs that provided the spacetime structure outside a rotating gravitational body. Thus, the spacetime so obtained by solving the EFEs involved two parameters, the mass M and angular momentum J of the spacetime, and it is known as Kerr spacetime. The line element is stationary, axisymmetric, and in Boyer–Lindquist coordinates, it can be expressed as [3, 4]

$$ds^2 = -\left(1-\frac{2Mr}{\Sigma}\right)dt^2+\frac{\Sigma}{\Delta}dr^2+\Sigma d\theta^2+\sin^2\theta\,\frac{(r^2+a^2)^2-a^2\Delta\sin^2\theta}{\Sigma}d\phi^2, \tag{1.8}$$

$$-\frac{4Mar\sin^2\theta}{\Sigma}d\phi\,dt, \tag{1.10}$$

where

$$\Delta = r^2-2Mr+a^2, \qquad \Sigma = r^2+a^2\cos^2\theta, \qquad a=\frac{J}{M}. \tag{1.9}$$

As in the case of the RNKB, the KBH also possesses two coordinate horizons, located at the roots of $\Delta = 0$, which comes from the condition $g_{rr} = 0$ (or equivalently, $1/g_{rr} = 0$) which on solving gives

$$r_\pm = M \pm \sqrt{M^2-a^2}. \tag{1.14}$$

Now, depending on the parameters M and a, the line element describes two horizons if $a \leq M$, and for $a = M$ the horizons coincide into a single horizon; in this case, the BH is said to be an extremal BH. If $a > M$, the horizons disappear, and the central singularity becomes visible, resulting in an NS.

Another important surface in the Kerr geometry is the *stationary limit surface* (SLS), defined by the vanishing of the g_{tt} component of the metric:

$$g_{tt} = -\left(1-\frac{2Mr}{\Sigma}\right) = 0. \tag{1.15}$$

Solving for r, we obtain the location of the stationary limit surface:

$$r_{\rm SLS}(\theta) = M+\sqrt{M^2-a^2\cos^2\theta}. \tag{1.16}$$

This surface lies outside the outer event horizon ($r_{\rm SLS} > r_+$ for $\theta \neq 0, \pi$) and coincides with the horizon at the poles. The region bounded between the event horizon and the stationary limit surface (shown by the gray region in Fig. [**?**]) is called the *ergosphere*.

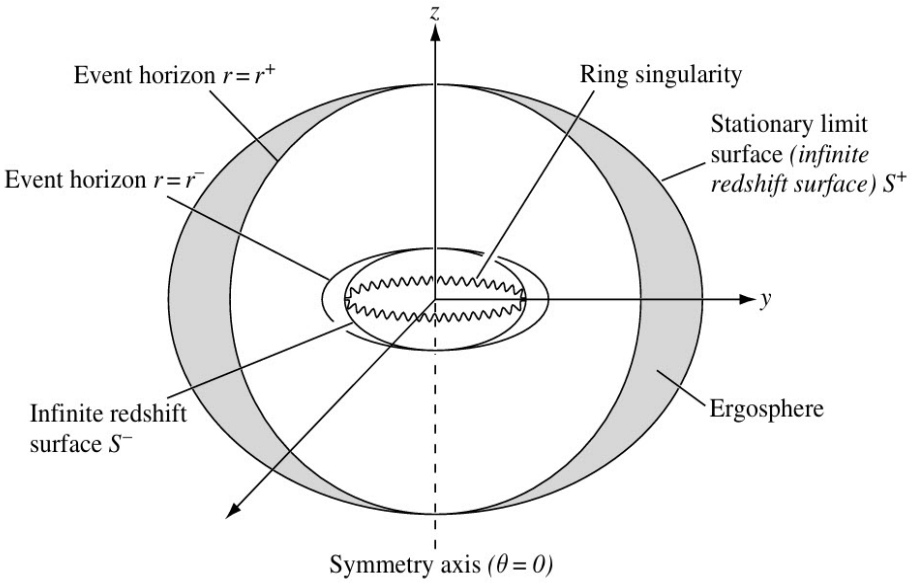

Figure 1.1: The Structure of the Kerr black hole.

Within the ergosphere, although particles can still escape to infinity, they cannot remain stationary with respect to a distant observer. This is because the timelike Killing vector ∂_t becomes spacelike inside the ergosphere, indicating that no static observer can exist there. Due to the frame-dragging effect, all objects are inevitably drawn into co-rotation with the black hole. This region is essential for energy extraction mechanisms such as the Penrose process.

The KBH also possesses a ring singularity at $\Sigma = 0$, that is, at $r = 0$, $\theta = \frac{\pi}{2}$, located in the equatorial plane. This is a real curvature singularity, where spacetime curvature becomes infinitely large.

Unlike the SBH and RNBH, the KBH is not static because the metric is not invariant under the transformation $t \mapsto -t$. Because the black hole rotates, Kerr spacetime loses its spherical symmetry and becomes merely axisymmetric. These characteristics give rise to a variety of rich and complex physical effects that distinguish rotating BHs from their non-rotating counterparts.

1.8 Kerr–Newman Black Hole

In 1965, Ezra T. Newman extended the Kerr solution to include electric charge, leading to the spacetime now known as the Kerr–Newman black hole (KNBH). This solution is stationary and axisymmetric, satisfying the coupled Einstein–Maxwell equations. It describes the spacetime

surrounding a rotating object that carries an electric charge. The black hole is fully specified by three parameters: its mass M, electric charge Q, and angular momentum J. In Boyer–Lindquist coordinates, the corresponding line element can be expressed as [**?**, **?**]: [3, 4]

$$ds^2 = -\frac{\Delta}{\rho^2}\left(dt - a\sin^2\theta\, d\phi\right)^2 + \rho^2 d\theta^2 + \frac{\rho^2}{\Delta}dr^2 + \frac{\sin^2\theta}{2}\left[-a\,dt + (r^2+a^2)\,d\phi\right]^2, \quad (1.28)$$

where

$$\rho^2 = r^2 + a^2\cos^2\theta, \qquad \Delta = r^2 - 2Mr + Q^2 + a^2, \qquad a = \frac{J}{M}. \quad (1.10)$$

The electromagnetic field associated with the KNBH is defined via the four-potential one-form:

$$A_\mu dx^\mu = -\frac{Qr}{\rho^2}\left(dt - a\sin^2\theta\, d\phi\right). \quad (1.29)$$

The KNBH possesses two horizons, which are obtained from the condition $\Delta = 0$, or equivalently from $1/g_{rr} = 0$. Solving this quadratic equation in r yields

$$r_\pm = M \pm \sqrt{M^2 - Q^2 - a^2}, \quad (1.30)$$

with the condition $Q^2 + a^2 \leq M^2$ to ensure the existence of real horizons. The surface at $r = r_+$ is the event horizon, while $r = r_-$ is the inner (Cauchy) horizon. If $Q^2 + a^2 > M^2$, the roots become complex and the line element instead represents a NS.

The stationary limit surface (SLS), where the time-time component of the metric vanishes ($g_{tt} = 0$), defines the boundary beyond which no observer can remain stationary. Setting $g_{tt} = 0$, we find

$$g_{tt} = -\left(1 - \frac{2Mr - Q^2}{\rho^2}\right) = 0, \quad (1.31)$$

which gives the location of the SLS as

$$r_{\rm SLS}(\theta) = M + \sqrt{M^2 - Q^2 - a^2\cos^2\theta}. \quad (1.32)$$

As with the Kerr BH, the region between the SLS given by $r_{\rm SLS}$ and the event horizon given by r_+ is called the *ergosphere*. Within this region, the timelike Killing vector $\partial/\partial t$ becomes spacelike, implying that no static observer can exist. Frame-dragging effects dominate this region and play a crucial role in energy extraction mechanisms [23].

The KNBH also has an essential ring singularity at $\Sigma = 0$, which occurs at $r = 0$ and $\theta = \frac{\pi}{2}$ in the equatorial plane. This singularity is similar to that of the KBH. When $Q = 0$, the KN metric reduces to the Kerr solution, and if $a = 0$, the RNBH is recovered. These limiting cases demonstrate the consistency of the KNBH as a unifying solution in general relativity [24].

1.9 Precession in Curved Spacetime: Geodetic and Lense-Thirring Effects

Precession refers to the change in orientation of the rotational axis of a spinning object over time. It is a well-known phenomenon in classical mechanics, such as the wobbling motion of a spinning top, where the axis traces out a conical surface due to external torques. In general relativity, precession has deeper implications due to the curvature and dynamics of spacetime itself.

1.9.1 Geodetic Precession

A *gyroscope* is a spinning object whose axis of rotation tends to maintain its orientation in an inertial frame. In general relativity, a small spinning test particle,effectively a gyroscope,experiences a gradual change in its spin axis as it moves through curved spacetime. This effect, known as *geodetic precession*, was first suggested by Willem de Sitter in 1916 [25].

According to general relativity, massive objects curve the spacetime around them, and all freely falling bodies,including gyroscopes,follow geodesics, the straightest possible paths in that curved geometry. While the gyroscope axis remains fixed in a locally inertial frame, its direction appears to change with respect to distant observers because the spacetime itself is curved.

To visualize this, consider a circle of radius $R = 400$ miles in flat (Euclidean) space. Its circumference is $2\pi R$. Now imagine inserting a massive object at the center of this circle, warping the surrounding spacetime. Even if the radial coordinate still reads R, the actual circumference will be slightly *less* than $2\pi R$,by approximately 1.1 inches. A gyroscope orbiting along this circle will experience a shift in the orientation of its spin axis due to this deviation from flat geometry. This precession caused solely by spacetime curvature is called *geodetic precession* [25].

1.9.2 Lense–Thirring Precession

In 1918, Josef Lense and Hans Thirring proposed that a *rotating* mass drags the spacetime around it, an effect now known as *frame dragging* or the *Lense-Thirring (LT) effect* [26, 27, 28]. This effect causes the local inertial frames near the rotating mass to be twisted in the direction of the rotation, much like a spoon swirling honey.

For a gyroscope orbiting a rotating massive object, this frame dragging induces an additional precession of its spin axis,distinct from geodetic precession. The resulting motion is known as *Lense-Thirring precession*. Although predicted shortly after the formulation of general relativity, the LT effect was extremely difficult to test experimentally due to the weak nature of frame dragging near Earth and the lack of observational evidence for BHs at the time.

In 1959, Stanford physicist Leonard Schiff proposed that frame dragging could be measured using precision gyroscopes in Earth orbit. Following this idea, Stanford University initiated an ambitious experiment in 1962. This eventually led to *Gravity Probe B*, a satellite launched by NASA in 2004, designed specifically to measure both geodetic and Lense-Thirring precession around Earth. The final results, announced in 2011, confirmed Einstein's predictions within experimental uncertainty [29].

1.10 MATHEMATICAL FRAMEWORK FOR GYROSCOPIC SPIN PRECESSION

This section outlines the mathematical tools required to analyze the spin precession of a test gyroscope within curved spacetime. Such an investigation is fundamental to understanding how both the curvature and the rotational properties of spacetime affect the orientation of a gyroscope's spin vector as it traverses a path. We start by deriving a generalized expression for spin precession before specializing the analysis for scenarios involving black holes.

To establish this, consider a test gyroscope associated with an observer who remains stationary by following a Killing trajectory, K, within a stationary spacetime. Based on previous work [22, 30], the frequency of spin precession is defined by the following expression:

$$\Omega_s = \frac{1}{2K^2} * (\tilde{K} \wedge d\tilde{K}) \tag{1.11}$$

In the above formula, the squared magnitude of the Killing vector is determined by:

$$K^2 = g_{00} + 2\Omega g_{0c} + \Omega^2 g_{cc}. \tag{1.12}$$

In the context of a stationary and axisymmetric spacetime, there exist two primary symmetries represented by a temporal Killing vector ∂_0 and an azimuthal Killing vector ∂_ϕ. A typical stationary observer follows a trajectory that is a linear combination of these two vectors, given

by:

$$K = \partial_0 + \Omega \partial_\phi \tag{1.13}$$

where Ω represents the observer's angular velocity. Because of the inherent symmetries of the spacetime, the metric coefficients do not depend on the x^0 and x^c coordinates. Consequently, the covector (one-form) linked to K is given by:

$$\tilde{K} = g_{0\nu}\, dx^\nu + \Omega\, g_{\gamma c}\, dx^\gamma. \tag{1.14}$$

In a four-dimensional spacetime setting, let the indices ν and γ be defined over the set $\{0, c, 2, 3\}$. By partitioning the expression into its temporal and spatial contributions, we can write:

$$\tilde{K} = \left(g_{00}\, dx^0 + g_{0c}\, dx^c + g_{0i}\, dx^i\right) + \Omega \left(g_{0c}\, dx^0 + g_{cc}\, dx^c + g_{ic}\, dx^i\right), \tag{1.15}$$

where the spatial index i takes the values 2 and 3. Within the ergoregion of a stationary, axisymmetric spacetime, the metric components g_{0i} and g_{ic} vanish, simplifying the above expression to:

$$\tilde{K} = \left(g_{00}\, dx^0 + g_{0c}\, dx^c\right) + \Omega \left(g_{0c}\, dx^0 + g_{cc}\, dx^c\right). \tag{1.16}$$

Taking the exterior derivative yields:

$$d\tilde{K} = \left(g_{00,k}\, dx^k \wedge dx^0 + g_{0c,k}\, dx^k \wedge dx^c\right) + \Omega \left(g_{0c,k}\, dx^k \wedge dx^0 + g_{cc,k}\, dx^k \wedge dx^c\right). \tag{1.17}$$

Substituting $\tilde{K}$ and $d\tilde{K}$ into the definition of spin precession and simplifying under the assumptions of stationarity and axisymmetry, we arrive at the generalized expression for the spin precession frequency:

$$\begin{aligned}\Omega_p = {} & \frac{\varepsilon^{ck\ell}}{2\sqrt{-g}\left(1 + 2\Omega\frac{g_{0c}}{g_{00}} + \Omega^2\frac{g_{cc}}{g_{00}}\right)} \times \\ & \left[\left(g_{0c,k} - \frac{g_{0c}}{g_{00}} g_{00,k}\right) + \Omega\left(g_{cc,k} - \frac{g_{cc}}{g_{00}} g_{00,k}\right) + \Omega^2\left(\frac{g_{0c}}{g_{00}} g_{cc,k} - \frac{g_{cc}}{g_{00}} g_{0c,k}\right)\right].\end{aligned} \tag{1.18}$$

For a spacetime that is both stationary and axisymmetric, using the coordinate basis $\{0, r, \theta, \phi\}$, Eq. (1.14) reduces to the following form:

$$\begin{aligned}\tilde{\Omega}_p = {} & \frac{1}{2\sqrt{-g}\left(1 + 2\Omega\frac{g_{0\phi}}{g_{00}} + \Omega^2\frac{g_{\phi\phi}}{g_{00}}\right)} \left[\sqrt{g_{rr}}\left(g_{0\phi,\theta} - \frac{g_{0\phi}}{g_{00}} g_{00,\theta}\right)\right. \\ & \left. + \Omega\left(g_{\phi\phi,\theta} - \frac{g_{\phi\phi}}{g_{00}} g_{00,\theta}\right) + \Omega^2\left(\frac{g_{0\phi}}{g_{00}} g_{\phi\phi,\theta} - \frac{g_{\phi\phi}}{g_{00}} g_{0\phi,\theta}\right)\right] \hat{r} \\ & + \left[\sqrt{g_{\theta\theta}}\left(g_{0\phi,r} - \frac{g_{0\phi}}{g_{00}} g_{00,r}\right) + \Omega\left(g_{\phi\phi,r} - \frac{g_{\phi\phi}}{g_{00}} g_{00,r}\right) + \Omega^2\left(\frac{g_{0\phi}}{g_{00}} g_{\phi\phi,r} - \frac{g_{\phi\phi}}{g_{00}} g_{0\phi,r}\right)\right] \hat{\theta}.\end{aligned} \tag{1.19}$$

In the special case when $\Omega = 0$, the expression reduces to:

$$\tilde{\Omega}_p\big|_{\Omega=0} = \frac{1}{2\sqrt{-g}}\left[-\sqrt{g_{rr}}\left(g_{0\phi,\theta} - \frac{g_{0\phi}}{g_{00}}g_{00,\theta}\right)\hat{r} + \sqrt{g_{\theta\theta}}\left(g_{0\phi,r} - \frac{g_{0\phi}}{g_{00}}g_{00,r}\right)\hat{\theta}\right]. \quad (1.20)$$

This formula is valid only outside the ergoregion and describes the Lense-Thirring precession frequency experienced by a test gyroscope due to the rotation of a general stationary and axisymmetric spacetime.

CHAPTER 2

SPIN PRECESSION EFFECTS OF KERR BLACK HOLES

The present chapter examines the characteristics of spin precession within the framework of Kerr spacetime by linking a test gyroscope to a stationary observer. For the remainder of this analysis, the term "spin precession" specifically denotes the motion of a gyroscope coupled with such an observer. This phenomenon provides a robust mechanism for differentiating between a Kerr black hole (KBH) and a neutron star (NS). In KBH geometries, the precession frequency exhibits divergent behavior as the observer nears the event horizon, a manifestation of the intense frame-dragging and spacetime curvature present in that region. Conversely, in the case of an NS, this quantity remains finite throughout the entirety of the spacetime, with the sole exception of the singularity itself [8].

Beyond the analysis of spin precession, we also investigate two related relativistic effects: the Lense-Thirring (frame dragging) effect and the geodetic precession frequency in Kerr geometry. These studies deepen our understanding of how the rotation of spacetime influences gyroscopic motion and further aid in distinguishing between the Kerr BH and NS configurations [30].

2.1 Spin Precession Frequency for Stationary Observers

This section focuses on the generalised spin precession as measured by a stationary observer in Kerr spacetime. The studies show that the intricate dependence of spin dynamics on the

rotation of the spacetime and provides a theoretical basis for discriminating between BHs and NSs. The formulation presented here follows the spin precession method introduced in Chapter 1.

The Kerr spacetime's line element in Boyer–Lindquist coordinates is given as [4]:

$$ds^2 = -\left(1-\frac{2Mr}{\rho^2}\right)dt^2 + \frac{\rho^2}{\Delta}dr^2 + \rho^2 d\theta^2 - \frac{4Mar\sin^2\theta}{\rho^2}dtd\phi + \left(r^2+a^2+\frac{2Mra^2\sin^2\theta}{\rho^2}\right)\sin^2\theta\, d\phi^2, \tag{2.1}$$

where

$$\rho^2 = r^2 + a^2\cos^2\theta, \quad \Delta = r^2 - 2Mr + a^2. \tag{2.2}$$

The horizon equation $(g_{rr})^{-1} = 0$ has the solution of the form

$$r_\pm = M \pm \sqrt{M^2 - a^2}, \tag{2.3}$$

Depending on the black hole parameter, the line element represents black hole or naked singularity if $a \leq M$ or $M < a$. In addition to the event horizons, the Kerr geometry possesses two important boundaries known as the stationary limit surfaces. These are defined by the condition $g_{tt} = 0$, and the corresponding equation is:

$$r^2 - 2Mr + a^2\cos^2\theta = 0. \tag{2.4}$$

Solving this yields the radii of the inner and outer stationary limit surfaces:

$$r_{s\pm} = M \pm \sqrt{M^2 - a^2\cos^2\theta}. \tag{2.5}$$

At the poles ($\theta = 0, \pi$), the stationary limit surface coincides with the event horizon. The region between the outer event horizon r_+ and the outer stationary limit surface r_{s+} is called the *ergosphere* [31]. Within this region, the dragging of inertial frames prevents any observer from remaining stationary relative to a distant inertial observer.

The determinant of the Kerr metric, which appears in many relativistic calculations, has the square root:

$$\sqrt{-g} = \rho^2 \sin\theta. \tag{2.6}$$

To distinguish between an NS and a BH, we analyse the spin precession in Kerr spacetime. Using the metric components $g_{\mu\nu}$ of the Kerr geometry, the general spin precession $\vec{\Omega}_p$ is derived as:

$$\vec{\Omega}_p = \frac{1}{C}\left[A\sqrt{\Delta}\cos\theta\,\hat{r} + B\sin\theta\,\hat{\theta}\right], \tag{2.7}$$

where $\hat{r}$ and $\hat{\theta}$ denote unit vectors in the directions of the corresponding coordinates, respectively, and Ω is the angular velocity of the observer [32]. The coefficients A, B and C are given by:

$$\begin{aligned} A = {} & 2aMr - \frac{\Omega}{8}\left[8r^2 + 8a^2r^2 + 16a^2Mr + 3a^4 + a^4\cos 4\theta + 4a^2(2\Delta - a^2)\cos 2\theta\right] \\ & + 2\Omega^2 a^3 Mr \sin^4\theta, \end{aligned} \tag{2.8}$$

$$\begin{aligned} B = {} & aM(r^2 - a^2\cos^2\theta) + \Omega\left[a^4 r\cos^4\theta + r^2(r^3 - 3Mra^2(1+\sin^2\theta))\right. \\ & \left. + a^2\cos^2\theta(2r^3 - Mr^2 + a^2M(1+\sin^2\theta))\right] \\ & + \Omega^2 aM\sin^2\theta\left[r^2(3r^2+a^2) + a^2\cos^2\theta(r^2-a^2)\right]. \end{aligned} \tag{2.9}$$

$$C = \rho^3\left[(\rho^2 - 2Mr) + 4\Omega Mar\sin\theta - \Omega^2\sin^2\theta\left\{3Ma^2r\sin^2\theta + \rho^2(r^2+a^2)\right\}\right]. \tag{2.10}$$

Note that here the angular velocity Ω plays a critical role in distinguishing a static observer from a stationary one. In the following subsection, we analyse the allowed range of Ω for stationary observers.

2.1.1 Range of Ω

Note that the general spin precession defined by Eq. (2.7) is valid for timelike observers, which may reside inside the ergoregion. Hence, Eq. (2.7) holds both inside and outside the ergoregion, but for a timelike observer, the following condition must be satisfied:

$$K^2 = g_{\phi\phi}\Omega^2 + 2g_{t\phi}\Omega + g_{tt} < 0. \tag{2.11}$$

This inequality is satisfied only when the angular velocity Ω at any fixed point (r,θ) lies within the range

$$\Omega_- < \Omega < \Omega_+, \tag{2.12}$$

where

$$\Omega_\pm = \frac{-g_{t\phi} \pm \sqrt{g_{t\phi}^2 - g_{\phi\phi}g_{tt}}}{g_{\phi\phi}}. \tag{2.13}$$

Using the metric components $g_{\mu\nu}$ from Eq. (2.1), this becomes

$$\Omega_\pm = \frac{2Mar\sin\theta \pm \rho^2\sqrt{\Delta}}{\sin\theta[\rho^2(r^2+a^2) + 2Ma^2r\sin^2\theta]}. \tag{2.14}$$

From this expression, it is can be seen that when the observer approaches the horizon (i.e., $\Delta \to 0$), the two limits $\Omega_\pm$ converge, and we have

$$\Omega_H = \frac{a}{2Mr_+}. \tag{2.15}$$

In the equatorial plane ($\theta = \pi/2$), Eq. (2.13) simplifies to

$$\Omega_\pm\Big|_{\theta=\frac{\pi}{2}} = \frac{2Ma \pm r\sqrt{\Delta}}{r(r^2+a^2)+2Ma^2}. \tag{2.16}$$

In the case of an NS, there is no horizon, and the ergoregion extends till the ring singularity. Further, in this plane the two limiting frequencies Ω_+ and Ω_- coincide at $r = 0$, the location of the singularity. Consequently, no stationary observer can exist at the event horizon for a black hole or at the ring singularity for a naked singularity. Therefore, the spin precession expression (2.13) is not valid exactly at these locations, although it remains valid in their vicinity [33].

To analyse the spin precession for various stationary observers, we parametrise the angular velocity Ω as

$$\Omega = q\Omega_+ + (1-q)\Omega_-, \tag{2.17}$$

and we can also rewrite this as

$$\Omega = \omega - (1-2q)\sqrt{\omega^2 - \frac{g_{tt}}{g_{\phi\phi}}}, \tag{2.18}$$

where $0 < q < 1$ and $\omega = -g_{t\phi}/g_{\phi\phi}$. Clearly, as $q \to 0$, $\Omega \to \Omega_-$, and as $q \to 1$, $\Omega \to \Omega_+$. Substituting the Kerr metric components, the angular velocity becomes

$$\Omega = \frac{2Mar\sin\theta - (1-2q)\rho^2\sqrt{\Delta}}{\sin\theta[2Ma^2 r\sin^2\theta + \rho^2(r^2+a^2)]}. \tag{2.19}$$

Thus, the full range of Ω between Ω_- and Ω_+ is smoothly covered as q varies from 0 to 1.

The spin precession frequency is then given by

$$\Omega_p = \frac{(r^2+a^2)^2 - a^2\Delta\sin^2\theta}{4q(1-q)\rho^7}\left[A\sqrt{\Delta}\cos\theta\,\hat{r} + B\sin\theta\,\hat{\theta}\right]. \tag{2.20}$$

The above expression provides the general form of spin precession, incorporating the effects of both spacetime rotation and curvature. It serves as a valuable tool for the upcoming discussion of black holes (BHs) and neutron stars (NSs). Moreover, the spin precession remains well-defined even within the ergosphere. In the following section, we will discuss two important types of spin precession: Lense-Thirring precession (arising due to rotation) and geodetic precession (arising due to curvature).

2.2 Lense-Thirring precession

Consider a test gyroscope in a rotating spacetime. If the gyroscope is orbiting around a central object, then after completing one full orbit, its axis of rotation will no longer point in the same direction as it did at the start of the motion. Instead, it changes its orientation due to the rotation of spacetime and this precession is Lense-Thirring (LT) precession, and it is sometimes referred to as the frame-dragging effect. To derive the expression for LT precession ($\Omega_{\rm LT}$) and understand its relation to spacetime rotation, we set $\Omega = 0$ in the general spin precession formula given by equation (2.20)

$$\vec{\Omega}_{\rm LT} = a\frac{2Mr\sqrt{\Delta}\cos\theta\hat{r} + M\left(r^2 - a^2\cos^2\theta\right)\hat{\theta}}{\left(r^2 + a^2\cos^2\theta\right)^{3/2}\left(r^2 - 2Mr + a^2\cos\theta\right)}, \tag{2.21}$$

The expression for LT precession diverges at the stationary limit surface, where the condition $r^2 - 2Mr + a^2\cos^2\theta = 0$ is satisfied. Furthermore, inside this surface, the spin precession formula is no longer valid. For this reason, to study the behaviour both inside the stationary limit surface and outside the event horizon, we have generalised the spin precession as given in equation (2.20). The spin precession frequency depends not only on the radial coordinate r, but also on the polar angle θ. To analyse how the spacetime rotation parameter affects the LT precession, we consider a gyroscope orbiting in the equatorial plane

$$\vec{\Omega}_{\rm LT}|_{\theta=\pi/2} = a\,\frac{Mr^2\,\hat{\theta}}{r^3(r^2 - 2Mr)} = a\,\frac{M\,\hat{\theta}}{r^3(1 - 2\frac{M}{r})}. \tag{2.22}$$

In the weak field approximation, that is, when $\frac{M}{r} \ll 1$, and by replacing $aM = J$, we can easily see that the magnitude of the LT precession becomes:

$$\Omega_{\rm LT} = \frac{J}{r^3}. \tag{2.23}$$

This shows that the LT precession is directly proportional to the angular momentum J of the black hole, and it decreases inversely with the cube of the radial distance.

2.3 Geodetic Precession in Schwarzschild Spacetime

In this section, we examine the phenomenon of geodetic precession induced by an SBH. By setting the rotation parameter $a = 0$ in the general expression for the spin precession of a KBH

[see Eq. (2.7)], the resulting precession arises solely due to the black hole's mass, rather than its spin. This mass-induced precession is known as *geodetic precession*

We consider the case when the rotation parameter vanishes ($a = 0$), leading to the following expression for spin precession:

$$\Omega_p\big|_{a=0} = \Omega \cdot \frac{-r\cos\theta\sqrt{r-2M}\,\hat{r} + \sin\theta(r-3M)\,\hat{\theta}}{r-2M-r^3\Omega^2\sin^2\theta}. \tag{2.24}$$

Here, Ω is constrained to values that ensure the four-velocity u remains within the timelike regime. Due to the spherical symmetry of Schwarzschild spacetime, this effect is the same for all values of θ. For simplicity, we restrict our analysis to the equatorial plane, where Eq. (2.24) reduces to:

$$\Omega_p\big|_{\theta=\pi/2,a=0} = \Omega\frac{r-3M}{r-2M-r^3\Omega^2}. \tag{2.25}$$

This implies that a gyroscope in motion within the static Schwarzschild spacetime experiences precession. For motion along a circular geodesic, Ω must match the Keplerian angular velocity, given by $\Omega_{\text{Kep}} = \sqrt{M/r^3}$. Substituting this into Eq. (2.25), we obtain:

$$\Omega_p\big|_{\Omega=\Omega_{\text{Kep}},a=0} = \Omega = \sqrt{\frac{M}{r^3}}. \tag{2.26}$$

In the Copernican frame, the above expression gives the precession frequency relative to proper time τ. In the coordinate system, the corresponding frequency is obtained by the relation $d\tau = \sqrt{1-\frac{3M}{r}}\,dt$, connecting the appropriate time τ and the coordinate time t. Therefore, the frequency in coordinate time is:

$$\Omega' = \sqrt{\frac{M}{r^3}}\sqrt{1-\frac{3M}{r}}. \tag{2.27}$$

The net angular displacement of the spin vector during a complete circuit is determined by calculating the difference between Ω and Ω':

$$\Omega_{\text{geodetic}} = \sqrt{\frac{M}{r^3}}\left(1-\sqrt{1-\frac{3M}{r}}\right). \tag{2.28}$$

This result reflects the geodetic precession Ω_{geodetic}, which arises solely due to the spacetime curvature caused by mass. This is consistent with characterisations in the literature [34]. This shows that the geodetic precession increases with increasing mass, as the spacetime curvature becomes stronger, and decreases with increasing radial distance.

2.4 Differentiating Kerr Naked Singularities from Black Holes via Gyroscopic Precession

The current section investigates the characteristics of spin precession for a variety of stationary observers. These observers are identified by their angular velocity Ω, which is defined using the parameter q. Following the formalism in [35], the scalar magnitude of the precession frequency, $\Omega_p = |\vec{\Omega}_p|$, is expressed as a function of the parameter q in the following manner:

$$\Omega_p = \frac{(r^2+a^2)^2 - a^2\Delta\sin^2\theta}{4a(1-q)\rho^7\Delta}\sqrt{A^2\Delta\cos^2\theta + B^2\sin^2\theta}, \tag{2.29}$$

where A and B are functions of Ω, defined in Eqs. (2.8) and (2.9). This expression is complex, so we analyse it graphically by plotting $|\Omega_p|$ as a function of r for different values of q. The spin precession frequency in the Kerr black hole spacetime is shown in Fig. 2.1, while for the NS case, it is depicted in Fig 2.1(b).

The graphical analysis demonstrates that Ω_p exhibits distinct behaviour in black hole and NS spacetimes. For KBHs, the spin precession Ω_p diverges at all the points near the event horizon for all observers except ZAMOs, who have $q = 0.5$ [see Fig. 2.1(c)]. In contrast, for Kerr naked singularities, Ω_p remains finite for all observers, even as $r \to 0$ at the equatorial plane.

Using the parameters a, q, r, and θ, we investigate the variation of the spin precession. From earlier results, it is evident that the denominator of Ω_p becomes zero when any of the conditions $\rho = 0$, $\Delta = 0$, or $q = 0, 1$ are met. Since the functions A and B remain finite. Ω_p diverges wherever its denominator approaches zero. Specifically, at the event horizon, that is where $\Delta = 0$ and at the ring singularity, where $\rho = 0$, at the horizon boundary, while $q = 0, 1$ correspond to the angular velocity limits.

Conversely, the right-hand panels of Fig. 2 indicate that for a Kerr NS with $a^* = 1.1$, the precession frequency remains finite across the entire domain, including as $r \to 0$ for $0 < \theta < \pi$. An exception occurs at the ring singularity point $r = 0, \theta = 90^\circ$, where Ω_p diverges. This sharply contrasts with the black hole case, where divergence occurs much farther from the centre, near the event horizon. Moreover, for $q > 0.5$, the appearance of local maxima and minima in Ω_p indicates additional structure that could assist in identifying the observer's angular velocity relative to the ZAMO.

We also observe that as Ω approaches its limiting values $\Omega_\pm$, the spin precession frequency Ω_p increases sharply. The figures in this study, ranging from Figure 1-4, illustrate the behaviour

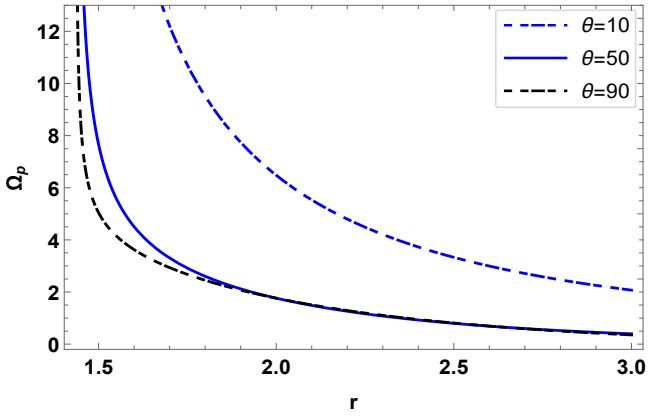

(a) $q = 0.1$

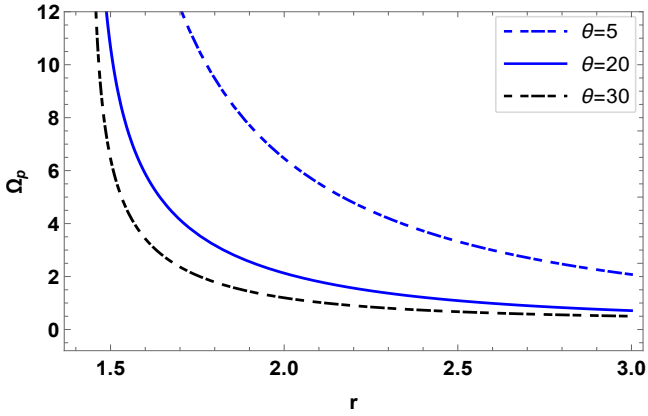

(b) $q = 0.5$ (ZAMO)

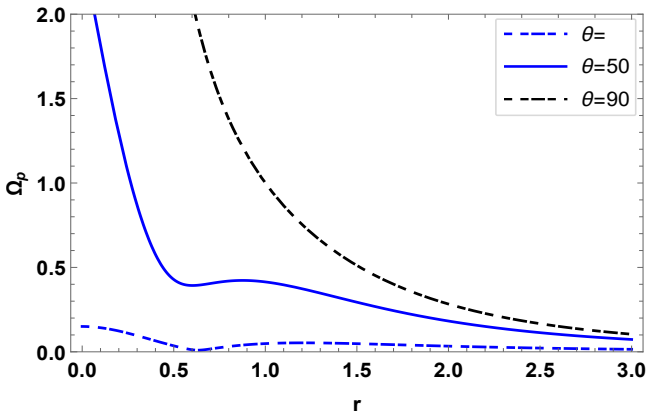

(c) $q = 0.9$

Figure 2.1: Spin precession Ω_p for a stationary observer in KBH spacetime ($a = 0.9$), shown for different angular velocity parameters q and angles θ.

of the spin precession frequency Ω_p for different values of the parameters q and the spin

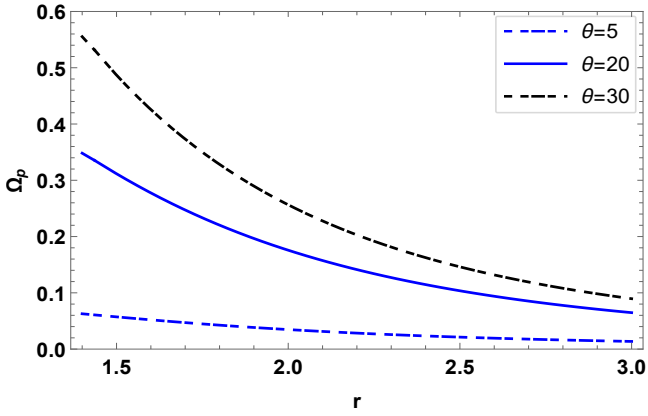

(a) $q = 0.1$

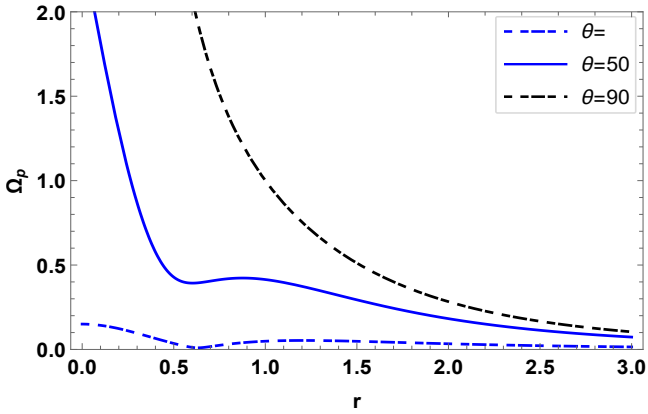

(b) $q = 0.5$ (ZAMO)

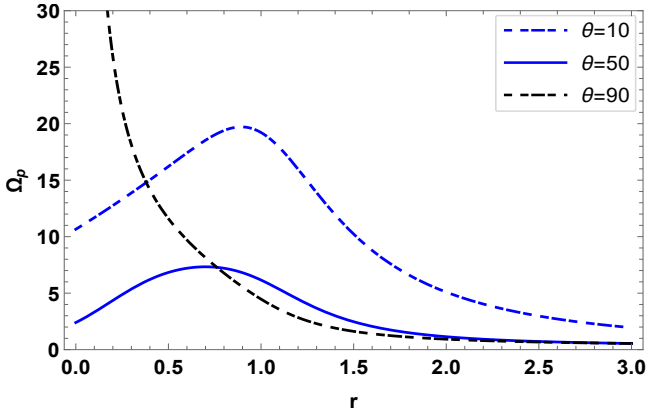

(c) $q = 0.9$

Figure 2.2: We have plotted the spin precession frequency of a stationary observer for different values of angular velocity in NS spacetime with rotational parameter $a = 1.1$, for different values of the angle θ.

a. Figures 1–3 show Ω_p for Kerr black holes and naked singularities with varying q and a,

highlighting that the precession remains regular inside and outside the ergoregion and diverges only at the horizon for most values of q. Figure 4 focuses on near-extremal and high-spin naked singularities, showing that Ω_p remains smooth across spacetime except near the ring singularity. Collectively, these figures provide a clear visual distinction between black holes and naked singularities and demonstrate the consistency of precession behaviour across different spin parameters and configurations.

CHAPTER 3

SPIN PRECESSION FREQUENCY OF KERR-LIKE BLACK HOLES

In this chapter, we investigate the effects of spin precession in Kerr-like black holes (KLBH) within the framework of Brans-Dicke theory, considering a cloud of strings and a perfect fluid background. We study spin precession as a means to distinguish BHs from NSs. As established in our earlier discussion in the previous chapter, gyroscopic precession for a KBH exhibits a singularity as the event horizon is approached. In contrast, for an NS, the precession frequency remains bounded throughout the entire spacetime, with the sole exception being the central singularity. Additionally, we examine the LT effect and geodetic precession frequencies in the spacetime of a KLBH to gain deeper insight into its unique gravitational characteristics.

3.1 Kerr-like Black Hole in Brans-Dicke Theory

The line element for a KLBH in Brans-Dicke theory is given by [36]:

$$ds^2 = \frac{1}{\psi(r,\theta)}\left[-\left(\frac{\Delta - a^2\sin^2\theta}{\rho^2}\right)dt^2 + \left(\frac{\left(r^2+a^2\right)^2 - a^2\Delta\sin^2\theta}{\rho^2}\right)\sin^2\theta d\phi^2\right]$$
$$-2\frac{a\sin^2\theta\left(r^2+a^2-\Delta\right)}{\psi(r,\theta)\rho^2}dtd\phi + \psi(r,\theta)\left[\frac{\rho^2}{\Delta}dr^2 + \rho^2 d\theta^2\right], \tag{3.1}$$

where

$$\Delta = r^2 - 2Mr + a^2, \tag{3.2}$$

$$\rho^2 = r^2 + a^2 \cos^2\theta, \tag{3.3}$$

and the scalar field ψ is defined as

$$\psi(r,\theta) = \Delta^{2/(2\omega+3)} \sin^{4/(2\omega+3)}\theta, \tag{3.4}$$

where the parameter ω lies in the range $-5/2 < \omega < -3/2$ [36]. We can see that the Kerr-like black hole in Brans-Dicke theory has two horizons, $r_\pm$ where Δ is given by Eq. (3.2), which can be obtained by solving $\Delta \equiv 0$. This gives the same horizon locations as in the Kerr black hole. Since these black holes also involve rotation, similar to the Kerr black hole, they are referred to as KLBH. It is evident that the line element (3.1) represents a BH with two horizons when $M > a$, and an NS when $M < a$. We verify this by studying spin precession in this spacetime, for which we need to calculate the spin precession frequency.

3.2 Spin Precession of rotating spacetime in Bran-Dicke theory

In this section, we analyze the spin precession Ω_p of the gyro in rotating spacetime Bran-Dicke theory . The precession frequency $\vec{\Omega}_p$ for rotating spacetime in Bran-Dicke theory. Substituting the metric components from (3.1) into (1.19) , we obtain:

$$\vec{\Omega}_p = \frac{1}{\sqrt{\psi}}\vec{\Omega}_p^{\text{Kerr}} = \frac{1}{C}\left[\left(A\sqrt{\Delta}\cos\theta\right)\hat{r} + (B\sin\theta)\,\hat{\theta}\right], \tag{3.5}$$

where

$$\begin{aligned} A = {} & 2aMr - \frac{\Omega}{8}\left[3a^4 + 8r^4 + 8a^2 r(2M+r) + a^2\left\{a^2\cos 4\theta + 4\left(2\Delta - a^2\right)\cos 2\theta\right\}\right] \\ & + 2Mr\Omega^2 a^3 \sin^4\theta, \end{aligned} \tag{3.6}$$

$$\begin{aligned} B = {} & aM\left(r^2 - a^2\cos^2\theta\right) + \Omega\left[a^4 r\cos^4\theta + r^2\left(r^3 - a^2 M\left(1+\sin^2\theta\right) - 3Mr^2\right)\right] \\ & + \Omega a^2\cos^2\theta\left\{2r^3 + a^2 M\left(1+\sin^2\theta\right) - Mr^2\right\} \\ & + aM\Omega^2\sin^2\theta\left[r^2\left(3r^2+a^2\right) + a^2\cos^2\theta\left(r^2 - a^2\right)\right], \end{aligned} \tag{3.7}$$

$$C = \rho^3\sqrt{\psi}\left[\rho^2 - 2Mr + 4\Omega arM\sin^2\theta - \Omega^2\sin^2\theta\left\{2Mra^2\sin^2\theta + \rho^2\left(r^2+a^2\right)\right\}\right]. \tag{3.8}$$

One should observe that as $\psi \to 1$, this relationship recovers the conventional spin precession formula for the KBH. Furthermore, the precession frequency described by Eq. (3.5) applies strictly to timelike observers maintained at constant r and θ. This requirement dictates a specific constraint on the observer's angular velocity, Ω:

$$\Omega_- < \Omega < \Omega_+, \tag{3.9}$$

where

$$\Omega_\pm = \frac{2Mra\sin\theta \pm \psi\rho^2\sqrt{\Delta}}{\sin\theta\left[(r^2+a^2)\rho^2 + 2Mra^2\sin^2\theta\right]}. \tag{3.10}$$

3.2.1 Lense-Thirring Precession Frequency

As discussed in the previous chapter, the formula for spin precession Ω_p given by Eq. (3.6) is a generalized expression that includes both Lense-Thirring as well as geodetic contributions. To isolate this frame-dragging part, as it arises due to the dragging of inertial frames, we set $\Omega = 0$ in Eq. (3.5). This yields the following expression:

$$\Omega_{\rm LT} = \frac{1}{2}\frac{\varepsilon_{ijl}}{\sqrt{-g}}\left[g_{0i,j}\left(\partial_l - \frac{g_{0l}}{g_{00}}\partial_0\right) - \frac{g_{0i}}{g_{00}}g_{00,j}\partial_l\right], \tag{3.11}$$

Since the KLBH in Brans-Dicke theory is stationary, the covector form of the precession frequency becomes:

$$\vec{\Omega}_{\rm LT} = \frac{1}{2\sqrt{-g}}\left[-\sqrt{g_{rr}}\left(g_{0\phi,\theta} - \frac{g_{0\phi}}{g_{00}}g_{00,\phi}\right)\hat{r} + \sqrt{g_{\theta\theta}}\left(g_{0\phi,r} - \frac{g_{0\phi}}{g_{00}}g_{00,r}\right)\hat{\theta}\right], \tag{3.12}$$

Using the metric components from equation (3.1), we obtain:

$$\vec{\Omega}_{\rm LT} = \frac{1}{\sqrt{\psi}}\Omega_{\rm LT}^{\rm Kerr} = \frac{aM}{\sqrt{\psi}}\frac{\left[\left(2r\sqrt{\Delta}\cos\theta\right)\hat{r} + \sin\theta\left(r^2 - a^2\cos^2\theta\right)\hat{\theta}\right]}{(\rho^2)^{3/2}\left(\rho^2 - 2Mr\right)}. \tag{3.13}$$

This generalizes the results for the KLBH, and we can see how it is related to the radial distance in the weak-field approximation, when $M/r \ll 1$. In the equatorial plane and under the weak-field approximation, the BD scalar field takes the form

$$\psi_{|\theta=\pi/2} \approx \frac{1}{r^{\frac{4}{2\omega+3}}}, \tag{3.14}$$

and hence the magnitude of the LT precession in the equatorial plane and weak field approximation takes the following form:

$$\vec{\Omega}_{{\rm LT}-weak} \propto \frac{J}{r^{\frac{6\omega+11}{2\omega+3}}}. \tag{3.15}$$

where J is the angular momentum of the spacetime. Now, we will discuss how it behaves near the ergosphere, as the formalism for the LT precession frequency is only valid outside the ergosphere.

3.3 Geodetic Precession

In this section, we analyze the geodetic precession frequency caused by a Schwarzschild-like (i.e., static) black hole in the presence of string cloud gravity. To do this, we set the rotation parameter $a = 0$ in the generalized spin precession expression for the Kerr-like black hole in Brans-Dicke theory given in Eq. (3.2.1), which yields:

$$\vec{\Omega}_p\Big|_{a=0} = \Omega\frac{(r-3M)\sin\theta\,\hat{\theta} - \sqrt{r^2-2Mr}\cos\theta\,\hat{r}}{\sqrt{\psi}\left[r-2M-r^3\Omega^2\sin^2\theta\right]}. \tag{3.16}$$

Here, Ω can take any value such that the observer's 4-velocity u remains timelike. Due to the spherical symmetry of the Schwarzschild-like spacetime in Brans-Dicke theory, we simplify the expression for the equatorial plane ($\theta = \pi/2$) as:

$$\vec{\Omega}_p = \frac{(r-3M)\hat{\theta}}{\sqrt{\psi}\,[r-2M-r^3\Omega^2]}. \tag{3.17}$$

The Keplerian frequency Ω_{Kep} for a particle orbiting in the equatorial plane of a black hole spacetime can be expressed in terms of the metric components as:

$$\Omega_{\text{Kep}} = \frac{g'_{t\phi} + \sqrt{(g'_{t\phi})^2 - g'_{tt}g'_{\phi\phi}}}{g'_{\phi\phi}}. \tag{3.18}$$

This implies that a gyroscope moving in a Schwarzschild-like spacetime will experience precession. When the gyroscope moves along a circular geodesic with angular frequency $\Omega = \Omega_{\text{Kep}}$, the expression in Eq. (3.3) evaluated at $\theta = \pi/2$ becomes:

$$\Omega_p\big|_{a=0,\Omega=\Omega_{\text{Kep}}} = \Omega = \left(\frac{M}{r^3}\right)^{1/2}. \tag{3.19}$$

This confirms that a gyroscope in a static Schwarzschild spacetime undergoes precession. For a circular geodesic path, the frequency of precession, denoted by Ω_{geodetic}, is:

$$\Omega_{\text{geodetic}} = \frac{1}{\sqrt{\psi}}\left(\frac{M}{r^3}\right)^{1/2}\left(1-\sqrt{1-\frac{3M}{r}}\right), \tag{3.20}$$

where it has been previously established that the sole contributor to this precession is the geodetic effect.

3.4 Distinguishing Naked Singularities from Kerr-like Black Holes

In this section, we investigate the behavior of the spin precession frequency for different stationary observers, where the angular velocity Ω is related to the parameter q. To do this, we express the magnitude of the spin precession frequency $\Omega_p = |\vec{\Omega}_p|$ as a function of the angular velocity parameter q, which can be written as:

$$\Omega_p = \frac{(r^2+a^2)^2 - a^2\Delta\sin^2\theta}{4a(1-q)\psi^2\rho^7\Delta}\sqrt{F^2\Delta\cos^2\theta + H^2\sin^2\theta}. \tag{3.21}$$

This equation describes the spin precession frequency for a Kerr-like black hole. If we set the parameters $\psi = 0$ and $\Delta = 0$, the spin precession becomes arbitrarily large when the denominator becomes singular. Notably, the terms F and H remain finite. This means that the spin precession is important to study.

In the previous plots, the spin parameter a was kept less than 1, with q and θ varied. Specifically, for the black hole case, a was assigned values such as $a = 0.6$, and the spin parameter q and angle θ were adjusted to examine how the spin precession frequency behaves under varying conditions. For naked singularities, however, a was chosen to exceed 1, marking a key distinction. In these cases, the values of q and θ were systematically varied as well.

The spin precession for different black hole and the naked singularity cases for different values of black hole parameters has been plotted in Fig-3.1 - 3.5. These results suggest that for naked singularities, the spin precession remains finite across all values of r, except at the ring singularity where the frequency diverges whereas for black hole it diverges as the observer approach the black hole horizons in all the directions.

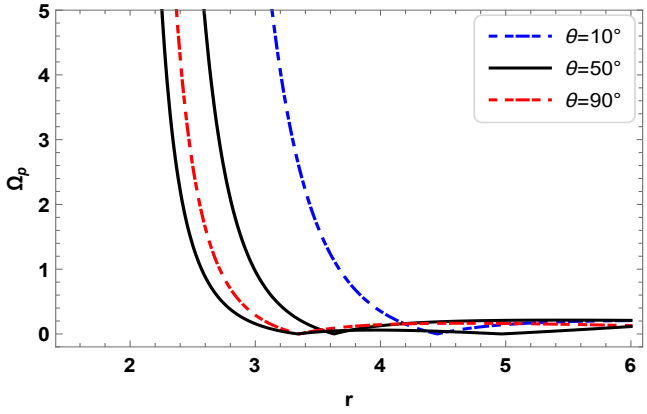

(a) $q = 0.1$

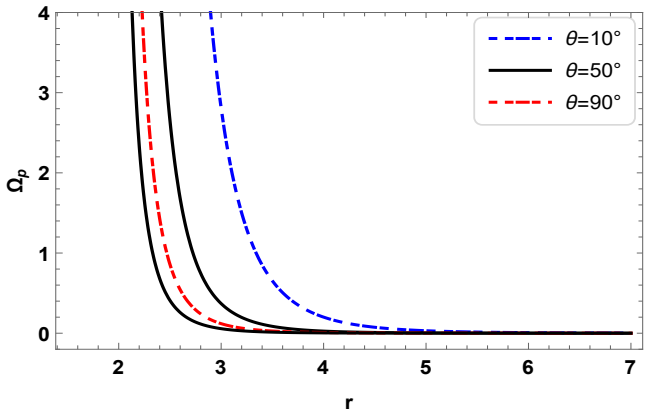

(b) $q = 0.5$ (ZAMO)

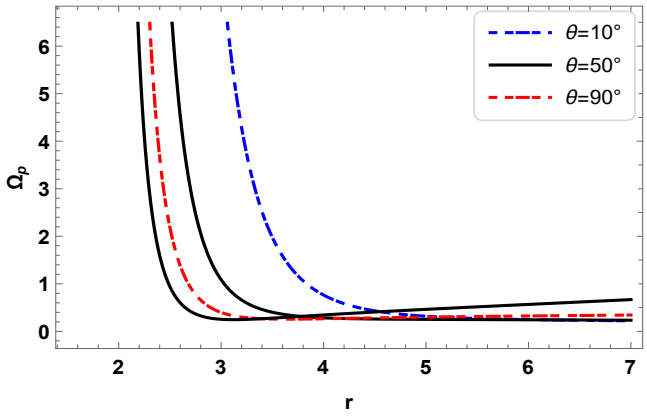

(c) $q = 0.9$

Figure 3.1: We have plotted the spin precession frequency of a stationary observer for different values of angular velocity in KBH spacetime with rotational parameter $a = 0.6$, for different values of the angle θ.

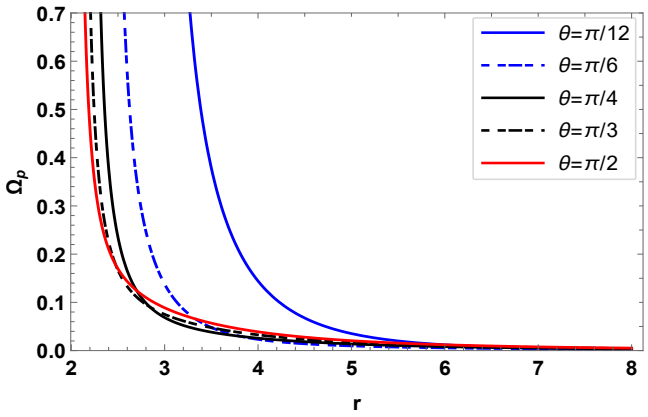

(a) $q = 0.1$

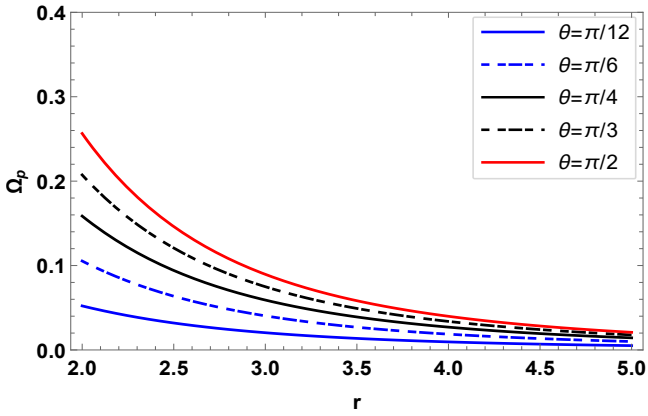

(b) $q = 0.5$ (ZAMO)

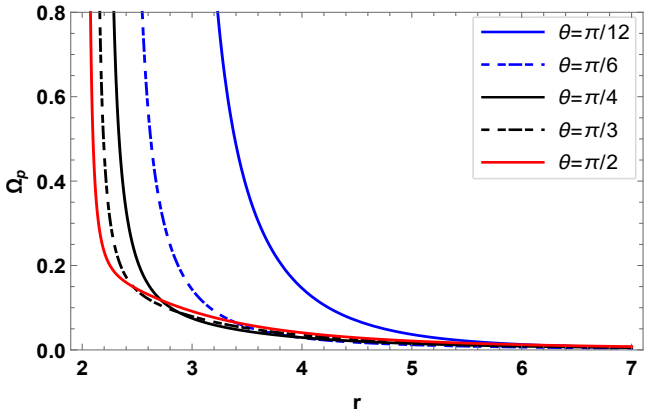

(c) $q = 0.9$

Figure 3.2: We have plotted the spin precession frequency in Kerr-like in Brans-Dicke gravity with rotational parameter $a = 0.9$, $\omega = -2$, for different values of the angle θ.

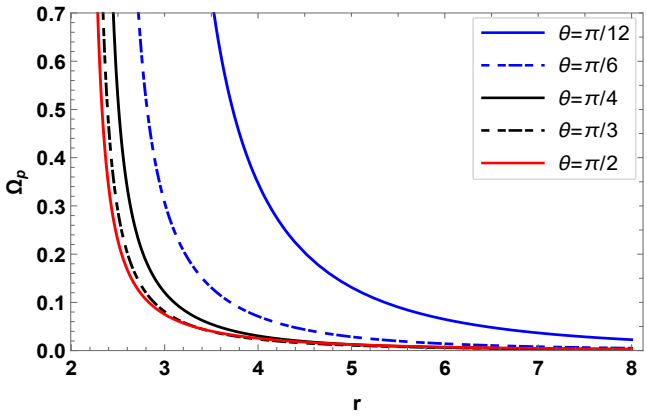

(a) $q = 0.1$

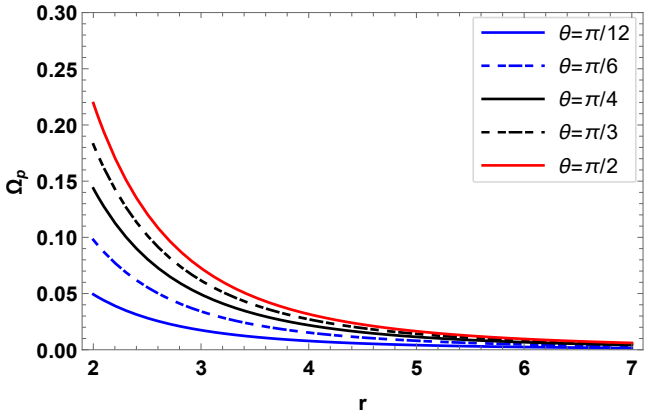

(b) $q = 0.5$ (ZAMO)

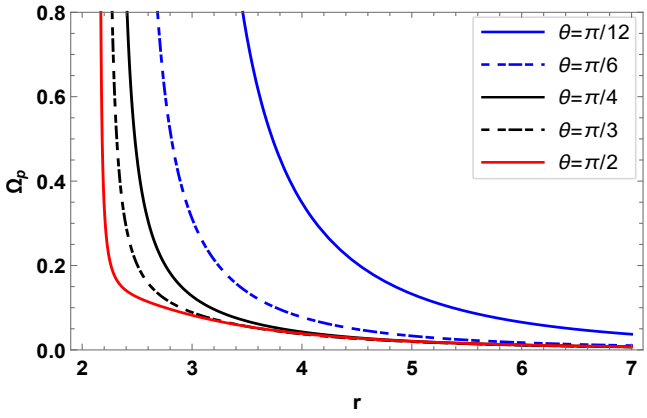

(c) $q = 0.9$

Figure 3.3: We have plotted the spin precession frequency in Kerr-like in Brans-Dicke gravity with rotational parameter $a = 0.7$, $\omega = -2.4$, for different values of the angle θ.

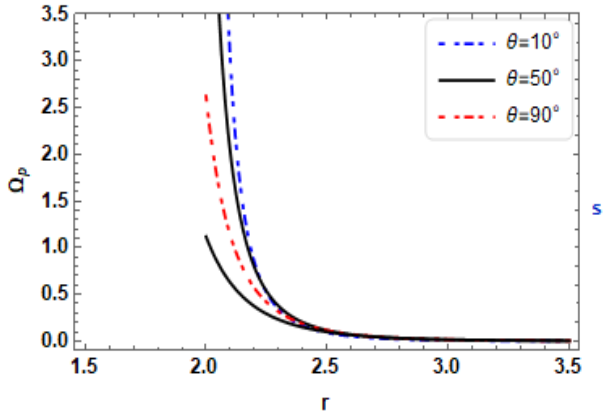

(a) $q = 0.1$

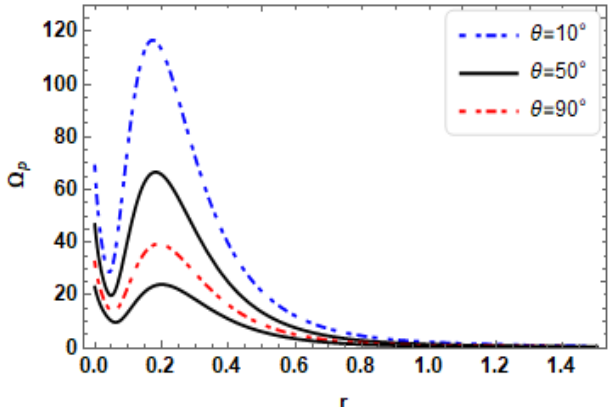

(b) $q = 0.5$ (ZAMO)

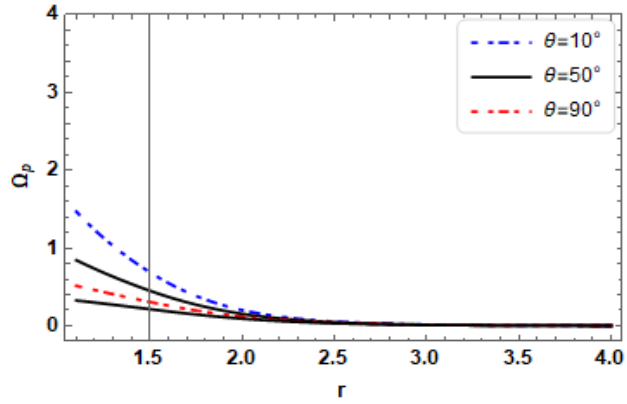

(c) $q = 0.9$

Figure 3.4: We have plotted the spin precession frequency of a stationary observer for different values of angular velocity, varying the parameter q, in KBH spacetime with rotational parameter $a = 0.9$ and for different values of θ.

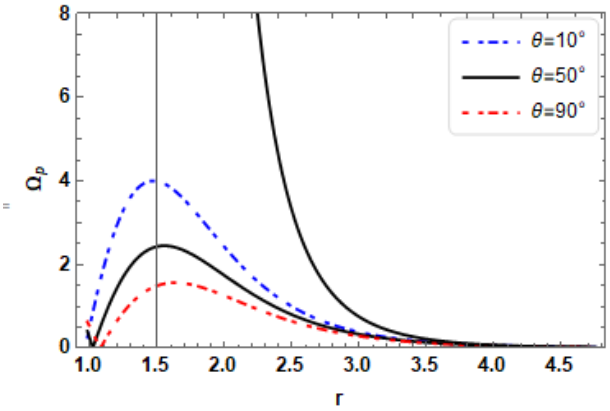

(a) $q = 0.1$

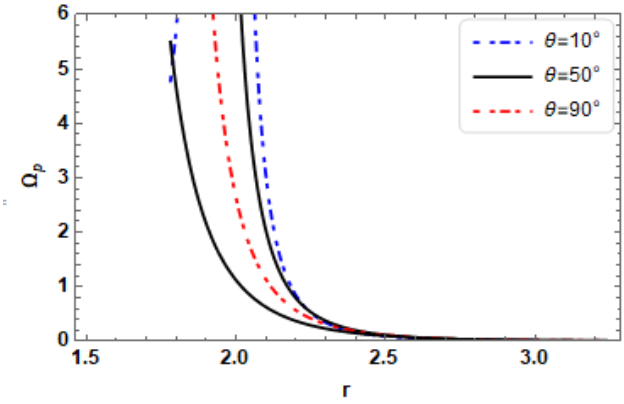

(b) $q = 0.5$ (ZAMO)

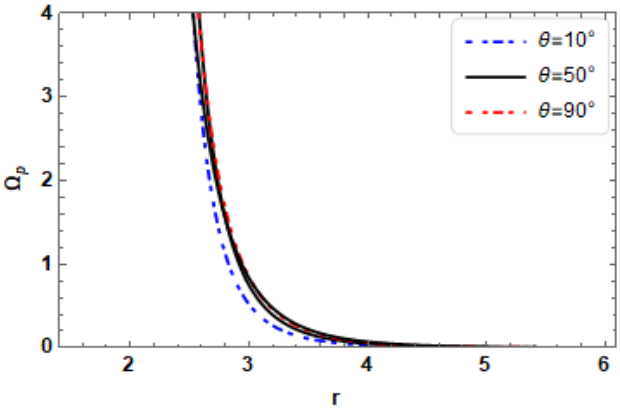

(c) $q = 0.9$

Figure 3.5: We have plotted the spin precession frequency of a stationary observer for different values of angular velocity, varying the parameter q, in the spacetime of a NS with a rotational parameter $a = 0.9$, considering various values of θ.

CHAPTER 4

BLACK HOLE WITH CLOUD OF STRINGS/GLOBAL MONOPOLE WITH DARK ENERGY

In this chapter, we investigate black holes with a cloud of strings and global monopoles in the presence of dark energy. A horizon analysis is carried out by examining the horizon equation and mapping the parameter space that differentiates black holes from naked singularities. To confirm these results, we further analyse the spin precession frequency in the corresponding spacetime, providing a consistent framework for validating the horizon structure. This study highlights the role of spin precession and examines how the presence of global monopoles and the dark energy parameter influences these effects, particularly in distinguishing black holes from naked singularities.

4.1 Black Hole with Cloud of Strings/Global Monopole with Dark Energy

In this section, we will study the The line element of the black hole with the cloud of strings with a perfect fluid background can be written [37]

$$ds^2 = -\left(\frac{\Delta - a^2\sin^2\theta}{\rho^2}\right)dt^2 - 2a\sin^2\theta\left(1 - \frac{\Delta - a^2\sin^2\theta}{\rho^2}\right)dtd\varphi + \frac{\rho^2}{\Delta}dr^2 + \rho^2 d\theta^2 + \sin^2\theta\left[\rho^2 + a^2\sin^2\theta\left(2 - \frac{\Delta - a^2\sin^2\theta}{\rho^2}\right)\right]d\varphi^2 \tag{4.1}$$

where the function

$$\Delta(r,\theta) = r^2 + a^2 - 2Mr - cr^2 + Q_E^2 + Q_M^2 - \frac{\alpha}{r^{3\omega-1}}.$$

Here, the parameters Q_E and Q_M represent electric and magnetic charge, c is the cloud string parameter, and α and ω are dark energy parameters. Depending on the values of spacetime, all these parameters, the line element (4.1) represents the BH or NS in other cases, but unlike the KBH case, the condition on the BH parameters in both cases is not as simple as in KBH, but we need very careful analysis of the horizon equation to get the parameter bounds to differentiate the BH and NS cases. For that purpose, we conducted a detailed horizon analysis.

4.2 Horizons Analysis

In this section to discussed the horizon geometry of the BH given by line element (4.1), we represents the radial distance and BH parameters in the units of BH gravitational mass M, that is, we replace $r/M \to r$, $a/M \to a$, $Q_E/M \to Q_E$, $Q_M/M \to Q_M$, and $\alpha/M \to \alpha$. Further, for simplicity, we suppose $b = 1-3\omega$ and $c = 8\pi\eta^2$. Thus, with this choice of units and notations, the BH horizons are roots of the horizon equation

$$\Delta = r^2 - 2r + a^2 - cr^2 + Q_E^2 + Q_M^2 - \alpha r^b = 0. \tag{4.2}$$

For any value of ω in the allowed range, the horizon equation has three real roots, repeated real roots and one real root and henceforth, the line element (4.1) represents a BH with three horizons, an extremal BH or a naked singularity, respectively.

Considering new parameter A a function of r and α as

$$A(r,\alpha) \equiv a^2 + Q_E^2 + Q_M^2 = 2r - (1-c)r^2 + \alpha r^b. \tag{4.3}$$

This parameter A has an extremal value for the dark matter parameter α as

$$\alpha_e = 2\left[\frac{(1-c)r-1}{br^{b-1}}\right]. \tag{4.4}$$

The extrema of this parameter is called the critical value α_c, and it is located at

$$r_e = \frac{(b-1)}{(b-2)(1-c)}. \tag{4.5}$$

Thus, the critical value of dark meter parameter α_c and the corresponding value of A_c are given as

$$\alpha_c = \frac{2}{b}\left(\frac{1-c}{b-1}\right)^{b-1}(b-2)^{b-2} \quad \text{and} \quad A_c(\alpha_c) \equiv a^2 + Q_E^2 + Q_M^2 = \frac{(b-1)}{b(b-2)(1-c)}. \tag{4.6}$$

In term of ω, we get

$$\alpha_c = \frac{2}{(1-3\omega)}\left(\frac{1-c}{-3\omega}\right)^{-3\omega}(-1-3\omega)^{-1-3\omega} \quad \text{and} \quad A_c(\alpha_c) = \frac{(-3\omega)^2}{(1-3\omega)(-1-3\omega)(1-c)}. \tag{4.7}$$

Thus, for any choice of parameter $-1 < \omega < -1/3$, the line element (4.1) can represent a BH only if $\alpha \leq a_c$ and the point (a, Q_E, Q_M) lies inside the sphere of radius A_c in aQ_EQ_M-space. Further, for $\alpha = \alpha_c$ and all points (a, Q_E, Q_M) on the surface of the sphere, the line element (4.1) represents an extremal BH with all horizons equal. In addition, if $\omega \to -1$, $\alpha_c \to 2(1-c)^3/27$, $A_c(\alpha_c) \to 9/8(1-c)$, that is, both α_c and A_c are finite. When $\omega \to -1/3$, $\alpha_c(\alpha) \to 1-c$ and $A_c(\alpha) \to \infty$, which means that a BH for very large values of a, Q_E and Q_M can be formed.

4.2.1 For $\omega = -2/3$

In this subsection, we will discuss the horizon equation (4.2) for $\omega = -2/3$. If the horizon equation (4.2) has three real roots, then (4.1) represents a BH with three horizons; if it has repeated real roots, then the line element represents an extremal BH, otherwise, it represents naked singularities. The horizon equation for $\omega = -2/3$ is

$$\Delta = r^2 - 2r + a^2 - cr^2 + Q_E^2 + Q_M^2 - \alpha r^3 = 0. \tag{4.8}$$

The extreme values of Δ can be obtained from the condition

$$\frac{d\Delta}{dr} = 2(1-c)r - 2 - 3\alpha r^2 = 0. \tag{4.9}$$

which gives their locations at

$$r_{\min} = \frac{1-c-\sqrt{(1-c)^2-6\alpha}}{3\alpha} \quad \text{and} \quad r_{\max} = \frac{1-c+\sqrt{(1-c)^2-6\alpha}}{3\alpha}, \tag{4.10}$$

For $\omega = -2/3$, $\alpha_c = (1-c)^2/6$, and for any value of $\alpha \leq \alpha_c$, we have real $r_{\min}$ and $r_{\max}$ and for $\alpha = \alpha_c$, $r_{\min} = r_{\max}$. Here $r_{\min}$ is minima and $r_{\max}$ is maxima of the Δ. The inner horizon r_-, outer horizons r_+, quintessential horizon r_q and extreme values of Δ are such that

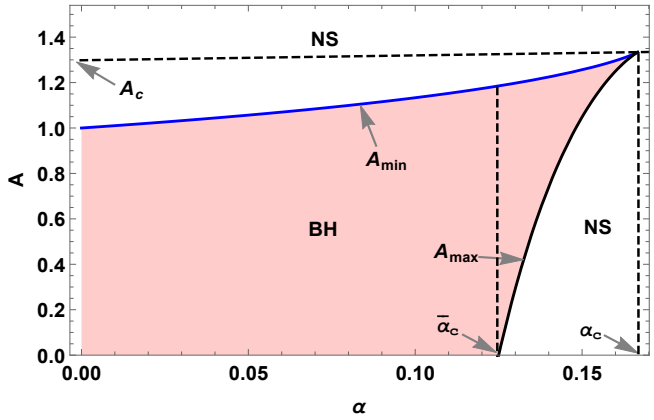

(a) $\omega = -2/3$, $c \approx 10^{-5}$ and $A = a^2 + Q_E^2 + Q_M^2$

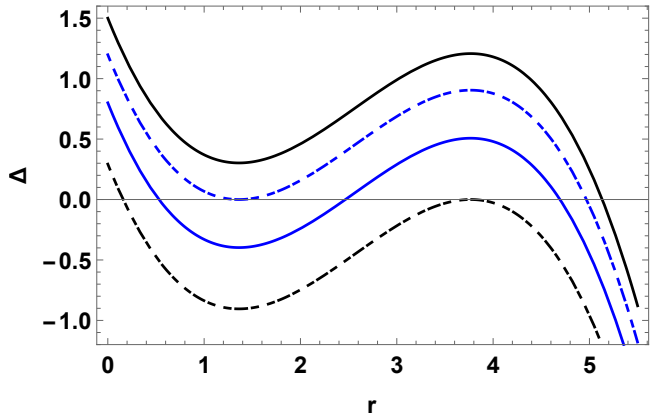

(b) $\alpha = 0.1$, $Q_E = 0.2$, $Q_M = 0.2$ (ZAMO)

Figure 4.1: (a) The region for the existence of a BH is plotted. The graphs show that the line element (4.1) represents a BH with three horizons for $\alpha \leq \overline{\alpha}_c$ if $A \leq A_{\min}$ and for $\overline{\alpha}_c < \alpha \leq \alpha_c$ if $A_{\max} \leq A \leq A_{\min}$ with $\overline{\alpha}_c \approx 0.1246$. Further, for any $\alpha \leq \alpha_c$, if $A = A_{\min}$ or $A = A_{max}$, then the the BH is extremal BH. (b) We have plotted Δ vs r (in units of M,) which shows a BH with three horizons (solid blue line), an extremal BH with $r_- = r_+$ (blue dashed line), an extremal BH with $r_+ = r_q$ (black dashed line) and a naked singularity (solid black line).

$r_- \leq r_{\min} \leq r_+ \leq r_{\max} \leq r_q$. Using the values of $r_{\min}$ and $r_{\max}$ in (4.2), we will get minimum and maximum value of the $A = a^2 + Q_E^2 + Q_M^2$ that are given by

$$A_{\min} = \frac{r_{\min}}{3}\left[4 - (1-c)r_{\min}\right] \quad \text{and} \quad A_{\max} = \frac{r_{\max}}{3}\left[4 - (1-c)r_{\max}\right]. \tag{4.11}$$

These values of A play an important role in differentiating a black hole from a naked singularity. For any $\alpha \leq \overline{\alpha}_c$ with $\overline{\alpha}_c \approx 0.1246$, the line element (4.1) represents black hole with three horizons if the point (a, Q_E, Q_M) lies inside the sphere of radius $A_{\min}$ and for $\overline{\alpha}_c < \alpha \leq a_c$ it represent black hole if the point (a, Q_E, Q_M) lies between the spheres of radius $A_{\min}$ and $A_{\max}$. This situation can be explained in FIG:(4.2). In FIG:(4.2)(a), the functions $A_{\min}$ and $A_{\max}$ are

plotted that separate BH solutions versus naked singular states. Within FIG:(4.2)(b) the horizons equation Δ for $\alpha = 0.13$ is plotted. The solid blue line is generated using $A = 0.8$, which represents the case of three-horizon BHs. The blue dashed line is plotted for $A = A_{\min}$, which represents an extremal BH where $r_- = r_+$ while the dark dashed line is plotted for $A = A_{\max}$, which corresponds to a degenerate BH state where $r_+ = r_q$. This solid dark-colored line plotted for $A > A_{\min}$ represents a naked singularity.

4.3 Lense-Thirring Precessional Shift

The present segment examines the Lense-Thirring (LT) gravitomagnetic effect frequency in the spacetime associated with a spinning BH influenced due to stringy cloud matter and dark energy. We derive the mathematical form for the LT frequency and analyze its behaviour in relation to various spacetime parameters. Furthermore, we present graphical plots depicting the LT behavior under varying the string cloud parameter, dark energy parameters, and the angular momentum of the BH. These plots help us understand how each parameter affects the frame-dragging effect and provide insights into distinguishing between BHs and NSs

$$\Omega_{\rm LT} = \frac{a}{\Sigma^{3/2}\left[\Sigma - (r^2 + a^2 - \Delta)\right]}\left[\sqrt{\Delta}\cos\theta(r^2 + a^2 - \Delta)\hat{r} + \sin\theta\left[M\left(r^2 - a^2\cos^2\theta\right)\right.\right.$$
$$\left.\left. - r\left(Q_E^2 + Q_M^2 + ca^2\cos^2\theta\right) + \frac{\alpha}{2}r^{b-1}\left\{(2-b)r^2 - ba^2\cos^2\theta\right\}\right]\hat{\theta}\right]. \tag{4.12}$$

The LT precession arises due to spacetime rotation and can be studied by calculating its magnitude

$$\Omega_{\rm LT} = \frac{a}{C}\left[A\hat{r} + B\hat{\theta}\right], \tag{4.13}$$

where

$$A = \sqrt{\Delta}\cos\theta(r^2 + a^2 - \Delta),$$
$$B = \sin\theta\left[M\left(r^2 - a^2\cos^2\theta\right) - r\left(Q_E^2 + Q_M^2 + ca^2\cos^2\theta\right) + \frac{\alpha}{2}r^{b-1}\left\{(2-b)r^2 - ba^2\cos^2\theta\right\}\right],$$
$$C = \rho^3\left[\Sigma - (r^2 + a^2 - \Delta)\right].$$

The magnitude of this the LT precession $|\Omega_{\rm LT}|$ is given as

$$|\Omega_{\rm LT}| = \frac{a}{|C|}(A^2 + B^2)^{\frac{1}{2}}. \tag{4.14}$$

Now, the results of the LT precession are plotted in Fig. 4.1- 4.4, which shows that if we consider the electric charge Q_E and increase it the LT precession frequency decreases. Also, we know the LT precession which is sometime called frame-dragging effect increases with the rotation parameter a increases reflecting the stronger frame-dragging effect associated with faster spinning black holes. In the similar way we can study effects of the dark energy parameter ω which shows increase in LT precession frequency, indicating the significant influence of dark energy on spacetime geometry. This analysis also locates regions where precession effects take over, providing insight into the relativistic physics occurring near the horizon.

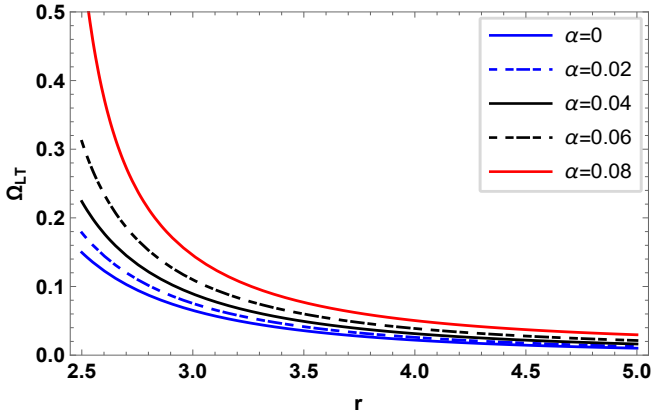

(a) $a = 0.6$, $Q_E = 0.2$, $Q_M = 0.2$

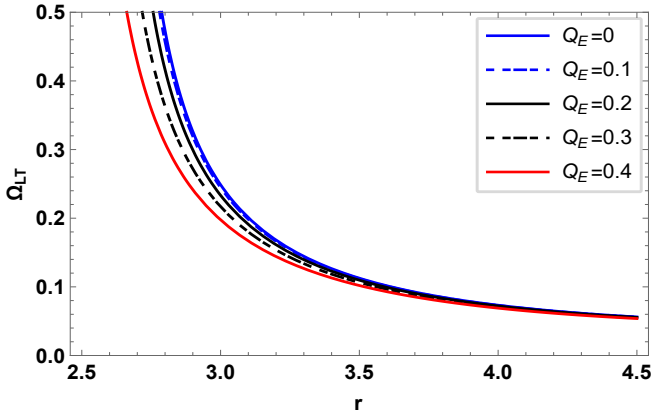

(b) $\alpha = 0.1$, $Q_E = 0.2$, $Q_M = 0.2$ (ZAMO)

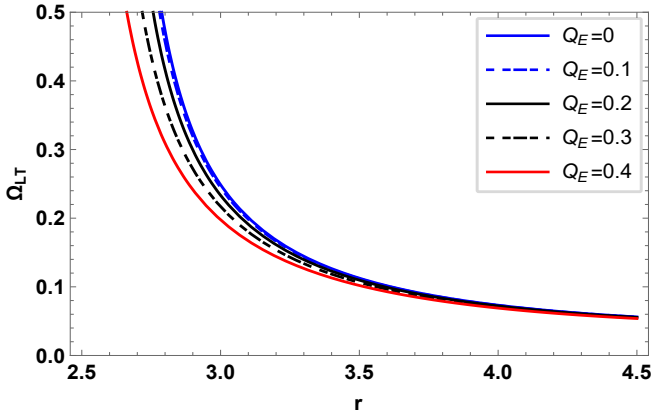

(c) $\alpha = 0.1$, $a = 0.6$, $Q_M = 0.2$

Figure 4.2: The LT precession frequency Ω_{LT} (in M^{-1}) verse r (in M) in the plane $\theta = \pi/4$ for $\omega = -2/3$, $c = 10^{-5}$ and different parameters is plotted.

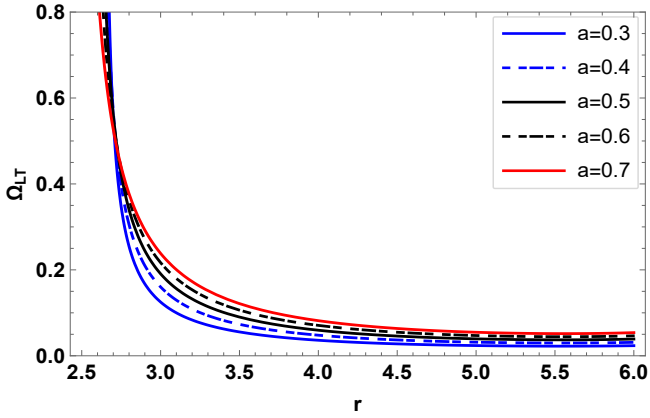

(a) , $\theta = \pi/6$

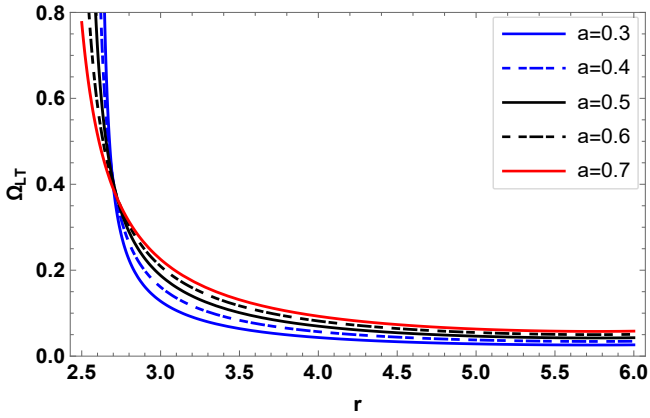

(b) $\theta = \pi/4$

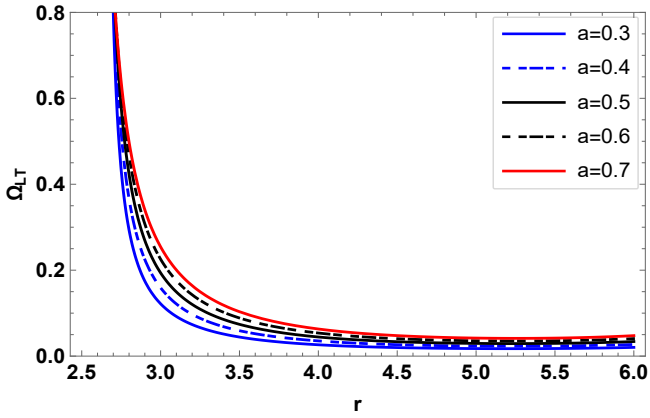

(c) $\theta = \pi/3$

Figure 4.3: The LT precession frequency Ω_{LT} (in M^{-1}) verse r (in M) in Kerr-like BH in cloud string and dark energy background with parameters $\alpha = 0.1$, $c = 10^{-5}$, $Q_M = 0.2$, $Q_E = 0.3$, $\omega = -2/3$, for different values of the angle a and θ.

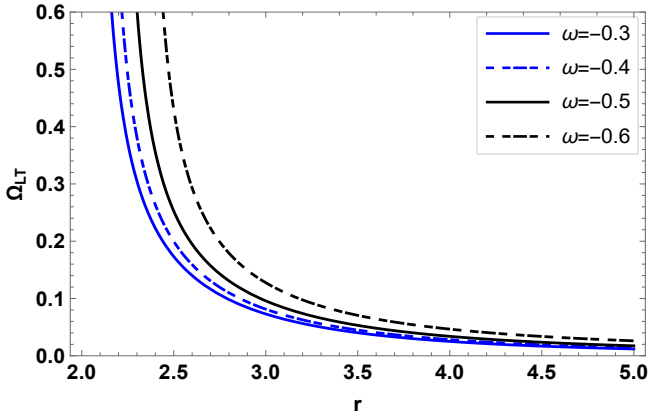

(a) $\theta = \pi/6$

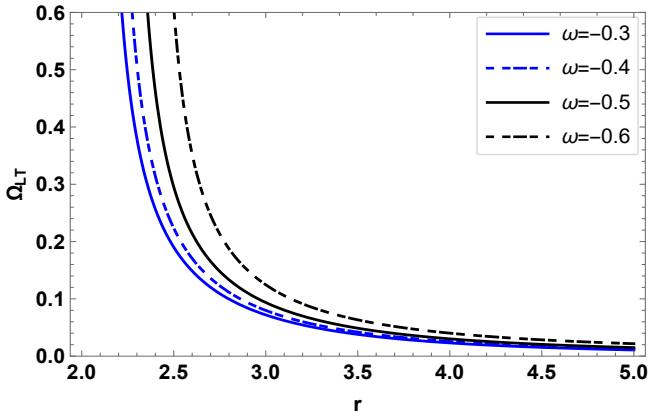

(b) $\theta = \pi/4$

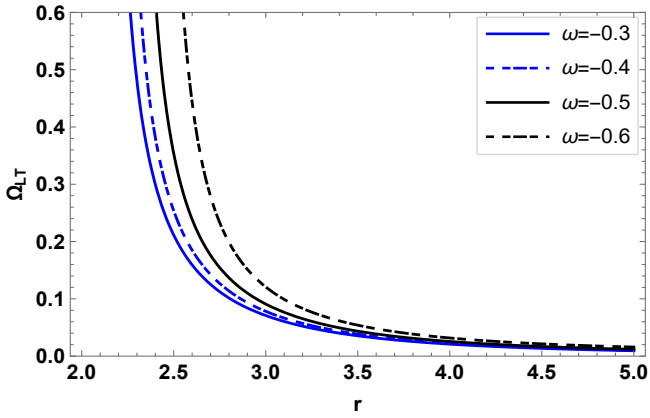

(c) $\theta = \pi/3$

Figure 4.4: The LT precession frequency $\Omega_{\rm LT}$ (in M^{-1}) verse r (in M) in Kerr-like BH in cloud string and dark energy background with parameters $\alpha = 0.1$, $c = 10^{-5}$, $Q_M = 0.2$, $Q_E = 0.3$, $a = 0.5$, for different values of the angle a and θ.

CHAPTER 5

CONCLUSION

5.1 Conclusion

In recent years, the challenge of distinguishing between black holes (BHs) and naked singularities (NSs) has gained significant attention in the field of gravitational physics. Understanding the final fate of gravitational collapse has long intrigued researchers, as it holds the key to unveiling the true nature of these extreme compact objects. In this thesis, we study the spin precession of test gyroscopes attached to test particles to differentiate Kerr-like black holes from naked singularities. We review the work for the standard Kerr black hole (KBH) and then extend the work to Kerr-like solutions within Brans–Dicke theory and a perfect fluid with a cloud of strings. The study of spin precession due to spacetime rotation and spacetime curvature has significant importance, and NASA has conducted the Gravity Probe B mission to measure these effects for Earth, which confirms that these effects are not just theoretical but that the measured values agree with predictions. In particular, differences in the behaviour of spin precession near black holes and naked singularities can serve as distinguishing markers, helping to address the long-standing cosmic censorship conjecture. Moreover, the sensitivity of gyroscopic motion to both the rotational and curvature-induced properties of spacetime makes it an invaluable probe for testing alternative theories of gravity. As observational precision improves with upcoming space missions and ground-based experiments, such precision-based diagnostics are expected to play an increasingly central role in the quest to uncover the true endpoints of gravitational

collapse.

5.2 Kerr-like Black Hole in Brans-Dicke Gravity

In this section, we summarise our findings on distinguishing BHs from NSs within the framework of Brans-Dicke gravity. This theory introduces a background scalar field characterised by the Brans-Dicke parameter ω. Our focus is on rotating BHs in Brans-Dicke gravity, specifically analysing a Kerr-like spacetime. The primary objective is to establish criteria that differentiate BHs from NSs in this context. The Kerr-like rotating BH features an additional parameter in its line element. Notably, the horizon equation for a KBH and that for a Kerr-like BH in Brans-Dicke gravity share the same form, enabling a direct comparison of the number and size of horizons.

In this work, we have studied spin precession effects arising from both spacetime rotation and curvature. These effects are significantly influenced by the Brans-Dicke parameter ω, which plays a critical role in altering the behaviour of test gyroscopes. We derived expressions demonstrating that geodetic precession explicitly depends on ω, and that spin precession is similarly affected. Notably, we use the nature of spin precession as a diagnostic tool to distinguish BHs from NSs in the Brans-Dicke framework. If the spin precession remains finite everywhere except in the case of a naked singularity, whereas it diverges as the observer approaches the event horizon in the case of a black hole, this distinction becomes evident through graphical analysis.

To further differentiate between black holes and naked singularities, we examined the angular velocity of observers, parameterised by a dimensionless factor k, where $k = 0.5$ corresponds to a Zero Angular Momentum Observer (ZAMO). The precession frequency of a test gyroscope was evaluated for stationary observers moving in opposite directions. A divergent precession frequency in all directions as the observer approaches the compact object indicates a BH spacetime. In contrast, if the precession remains finite in most directions, the object is identified as a naked singularity. This behaviour stems from the nature of the horizon: black holes exhibit infinite precession near the horizon in all directions, whereas naked singularities display such divergence only along the equatorial plane ($\theta = \pi/2$).

Through this analysis, we demonstrate that spin precession serves as a powerful probe for understanding the geometric structure and horizon properties of exotic astrophysical objects in modified gravity theories.

5.3 Kerr-like Black in Cloud String and dark energy

In this section, we summarise our findings on distinguishing BHs from NSs in a space-time influenced by a cloud of strings and dark energy. This extended framework incorporates additional physical features,namely, a string cloud parameter c and dark energy parameters α and ω,which modify the underlying geometry of the Kerr-like rotating black hole. These modifications introduce new degrees of freedom into the metric, offering a richer structure to study the nature of compact objects.

This study analyzes a rotating black hole embedded in a background influenced by dark energy and a cloud of strings, showing how these factors modify the horizon structure and causal boundaries. By determining critical parameter values, the work distinguishes black holes from naked singularities and identifies the conditions for extremal black holes. Additionally, the study examines how spacetime rotation and curvature affect spin precession, deriving analytical expressions for geodetic and Lense–Thirring precession. These spin precession features are shown to be sensitive probes for differentiating black holes from naked singularities in modified spacetimes.

5.4 Future Work

This research work has been conducted for the class of Kerr-like rotating spacetimes with spherically symmetric horizon structures, considering different background fields, particularly to differentiate black holes from naked singularities. It would also be worthwhile to study spin precession and use it to analyze the structure of black holes and naked singularities by incorporating NUT parameters and other scalar fields; for instance, this would clarify how specific geometric structures help differentiate black holes from naked singularities. Additionally, studying cylindrically symmetric solutions, sometimes called black strings, would allow us to examine whether spin precession remains an effective diagnostic tool in non-spherical geometries, and investigating higher-dimensional spacetimes would enable us to test the consistency of spin precession as a probe within modified gravity frameworks. Such research would ultimately deepen our understanding of how compact objects behave across a diverse array of gravitational

settings.

BIBLIOGRAPHY

[1] S. W. Hawking and L. Mlodinow, *A Briefer History of Time*. Bantam Press London, UK, 2020.

[2] A. Einstein, "The General Theory of Relativity," in *The Meaning of Relativity*. Springer, 1922.

[3] C. W. Misner, K. S. Thorne, and J. A. Wheeler, *Gravitation*. Princeton University Press, 2017.

[4] A. Qadir, *Einstein's General Theory of Relativity*. Cambridge Scholars Publishing, 2020.

[5] J. Michell, "On the Means of Discovering the Distance, Magnitude, & *c*. of the Fixed Stars, in Consequence of the Diminution of the Velocity of Their Light, in Case Such a Diminution Should be Found to Take Place in Any of Them, and Such Other Data Should be Procured From Observations, as Would be Farther Necessary for That Purpose. By the Rev. John Michell, BDFRS in a Letter to Henry Cavendish, Esq. FRS and AS," *Philosophical Transactions of the Royal Society of London*, vol. **74**, p. 35, 1784.

[6] C. Montgomery, W. Orchiston, and I. Whittingham, "Michell, Laplace and the Origin of the Black Hole Concept," *Journal of Astronomical History and Heritage*, vol. **12**, p. 90, 2009.

[7] S. W. Hawking and G. F. R. Ellis, *The Large Scale Structure of Spacetime*. Cambridge University Press, 1973.

[8] B. Chakraborty and A. Majumdar, "On Galilean Covariance in a Nonrelativistic Model Involving a Chern–Simons Term," *Annals of Physics*, vol. 250, no. 1, pp. 112–144, 1996.

[9] E. H. T. Collaboration *et al.*, "First M87 Event Horizon Telescope Results. I. The Shadow of the Supermassive Black Hole," *Astrophysical Journal Letters*, vol. 875, no. L1, 2019.

[10] S. Chandrasekhar, "The Maximum Mass of Ideal White Dwarfs," *Astrophysical Journal, vol. 74, p. 81*, vol. 74, p. 81, 1931.

[11] V. Frolov and I. Novikov, *Black Hole Physics: Basic Concepts and New Developments*. Springer Science & Business Media, 2012, vol. 96.

[12] A. Einstein, "On a Stationary System with Spherical Symmetry Consisting of Many Gravitating Masses," *Annals of Mathematics*, pp. 922–936, 1939.

[13] J. R. Oppenheimer and G. M. Volkoff, "On Massive Neutron Cores," *Physical Review*, vol. **55**, no. 4, p. 374, 1939.

[14] J. R. Oppenheimer and H. Snyder, "On Continued Gravitational Contraction," *Physical Review*, vol. **56**, no. 5, p. 455, 1939.

[15] E. E. Salpeter, "Accretion of Interstellar Matter by Massive Objects," 1965.

[16] Y. B. Zel'Dovich, "The Fate of a Star and the Evolution of Gravitational Energy Upon Accretion," in *Soviet Physics Doklady*, vol. 9, 1964, p. 195.

[17] S. Bowyer, E. Byram, T. A. Chubb, and H. Friedman, "Cosmic X-Ray Sources," *Science*, vol. 147, no. 3656, pp. 394–398, 1965.

[18] B. P. Abbott *et al.*, "GW151226: Observation of Gravitational Waves from a 22-Solar-Mass Binary Black Hole Coalescence," *Physical Review Letters*, vol. 116, no. 24, p. 241103, 2016.

[19] B. P. Abbott, R. Abbott, T. D. Abbott, M. R. Abernathy, F. Acernese, K. Ackley, C. Adams, T. Adams, P. Addesso, R. X. Adhikari *et al.*, "Observation of Gravitational Waves from a Binary Black Hole Merger," *Physical Review Letters*, vol. 116, no. 6, p. 061102, 2016.

[20] P. S. Joshi, "Gravitational Collapse and Spacetime Singularities," 2007.

[21] J. B. Hartle, *Gravity: An Introduction to Einstein's General Relativity*. Cambridge University Press, 2021.

[22] C. Chakraborty, P. Kocherlakota, M. Patil, S. Bhattacharyya, P. S. Joshi, and A. Królak, "Distinguishing Kerr Naked Singularities and Bblack Holes using the Spin Precession of a Test Gyro in Strong Gravitational fields," *Physical Review D*, vol. **95**, p. 084024, 2017.

[23] R. M. Wald, "On Perturbations of a Kerr Black Hole," *Journal of Mathematical Physics*, vol. 14, no. 10, pp. 1453–1461, 1973.

[24] J. Zhang and Z. Zhao, "New Coordinates for Kerr–Newman Black Hole Radiation," *Physics Letters B*, vol. 618, no. 1-4, pp. 14–22, 2005.

[25] W. De Sitter, "On Einstein's Theory of Gravitation and its Astronomical Consequences," *Monthly Notices of the Royal Astronomical Society*, vol. **77**, p. 155, 1916.

[26] H. Thirring, "On the Effect of Rotating Distant Masses in Einstein's Theory of Gravitation." *Physical. Z*, vol. **19**, 1918.

[27] B. Mashhoon, F. W. Hehl, and D. S. Theiss, "On the Gravitational Effects of Rotating Masses: The Thirring-Lense Papers," *General Relativity and Gravitation*, vol. **16**, p. 711, 1984.

[28] L. I. Schiff, "Possible New Experimental Test of General Relativity Theory," *Physical Review Letters*, vol. **4**, p. 215, 1960.

[29] C. F. Everitt *et al.*, "Gravity Probe B: Final Results of a Space Experiment to Test General Relativity," *Physical Review Letters*, vol. **106**, p. 221101, 2011.

[30] M. Rizwan, M. Jamil, and K. Jusufi, "Distinguishing a Kerr-like Black Hole and a Naked Singularity in Perfect Fluid Dark Matter via Precession Frequencies," *Physical Review D*, vol. 99, no. 2, p. 024050, 2019.

[31] C. Chakraborty, P. Kocherlakota, and P. S. Joshi, "Spin Precession in a Black Hole and Naked Singularity Spacetimes," *Physical Review D*, vol. 95, no. 4, p. 044006, 2017.

[32] C. Chakraborty and P. Majumdar, "Strong Gravity Lense–Thirring Precession in Kerr and Kerr–Taub–Nut Spacetimes," *Classical and Quantum Gravity*, vol. 31, no. 7, p. 075006, 2014.

[33] Z. Xu, X. Hou, and J. Wang, "Kerr–anti-de Sitter/de Sitter Black Hole in Perfect Fluid Dark Matter Background," *Classical and Quantum Gravity*, vol. 35, no. 11, p. 115003, 2018.

[34] K.-i. Sakina and J. Chiba, "Parallel Transport of a Vector Along a Circular Orbit in Schwarzschild Spacetime," *Physical Review D*, vol. **19**, p. 2280, 1979.

[35] C. Chakraborty, P. Kocherlakota, M. Patil, S. Bhattacharyya, P. S. Joshi, and A. Królak, "Distinguishing Kerr naked singularities and black holes using the spin precession of a test gyro in strong gravitational fields," *Physical Review D*, vol. 95, no. 8, p. 084024, 2017.

[36] H. Kim, "New Black Hole Solutions in Brans-Dicke Theory of Gravity," *Physical Review D*, vol. 60, no. 2, p. 024001, 1999.

[37] K. Jusufi, M. Jamil, P. Salucci, T. Zhu, and S. Haroon, "Black Hole Surrounded by a Dark Matter Halo in the M87 Galactic Center and its Identification with Shadow Images," *Physical Review D*, vol. 100, no. 044012, 2019.